NASA CONTRACTOR REPORT

A STUDY OF PANEL FLUTTER WITH THE EXACT METHOD OF ZEYDEL

by J. E. Yates

Prepared by
AERONAUTICAL RESEARCH ASSOCIATES OF PRINCETON, INC.
Princeton, N. J. 08540
for George C. Marshall Space Flight Center

NATIONAL AERONAUTICS AND SPACE ADMINISTRATION • WASHINGTON, D. C. • DECEMBER 1970

1. Report No.	2. Government Accession No.	3. Recipient's Catalog No.
NASA CR-1721		

4. Title and Subtitle	5. Report Date
A STUDY OF PANEL FLUTTER WITH THE EXACT METHOD OF ZEYDEL	December 1970
	6. Performing Organization Code

7. Author(s)	8. Performing Organization Report No.
J. E. Yates	ARAP Report No. 145
	10. Work Unit No.

9. Performing Organization Name and Address	11. Contract or Grant No.
Aeronautical Research Associates of Princeton, Inc. 50 Washington Road Princeton, New Jersey 08540	NAS8-24390
	13. Type of Report and Period Covered
12. Sponsoring Agency Name and Address	CONTRACTOR REPORT
NASA-George C. Marshall Space Flight Center Aero-Astrodynamics Laboratory Marshall Space Flight Center, Alabama 35812	14. Sponsoring Agency Code

15. Supplementary Notes

16. Abstract

The exact method of Zeydel for calculating flutter boundaries and estimating stresses in an infinite spanwise array of panels is presented. The theory is based on the exact linearized inviscid aerodynamic theory. A general analysis of orthotropic panels is presented that accounts for different edge conditions, elastic foundation, membrane stresses, and viscous and structural damping. Various asymptotic results are presented for very long panels. Two limits of the exact theory are discussed that correspond to the simple static aerodynamic theory approximation and the traveling-wave theory, respectively. A further result for the mode shape of a semi-infinite panel is presented that shows how a traveling wave is amplified and reflected by the trailing edge.

Extensive numerical calculations are presented for the special case of pinned edge panels, isotropic panel material, zero viscous damping, and no elastic foundation. Comparisons are made with previous results that verify the computational procedure. Design flutter boundaries are presented of mass ratio versus length-to-width ratio for different materials and altitude. Typical mode shapes are also given. The effect of structural damping at different Mach numbers and length-to-width ratios is discussed. Example calculations of the stress level in a panel are made.

Design flutter boundaries are presented for aluminum panels on a typical Saturn V trajectory. Flutter is indicated for certain panels on the forward skirt of the S-IVB stage, in agreement with in-flight data. Because of the relatively short duration of flutter, it is concluded that failure is not likely to occur.

1. Flutter

17. Key Words (Suggested by Author(s))	18. Distribution Statement
	Unclassified - Unlimited

19. Security Classif. (of this report)	20. Security Classif. (of this page)	21. No. of Pages	22. Price*
Unclassified	Unclassified	88	$3.00

*For sale by the Clearinghouse for Federal Scientific and Technical Information
Springfield, Virginia 22151

PREFACE

This report covers work initiated by the National Aeronautics and Space Administration, George C. Marshall Space Flight Center, Huntsville, Alabama under Contract NAS8-24390. The work was administered by Mr. R. G. Beranek.

The report covers the one-year period 19 May 1969 to 18 May 1970. The Principal Investigator was Dr. John E. Yates.

The author wishes to thank Mr. Beranek for his liaison work in getting computer runs submitted on the Marshall Space Flight Center facilities. The careful typing of the manuscript by Mrs. Lois Ridgway and Mrs. Joan Bugher and preparation of the drawings by Mrs. Patricia Tobin is gratefully acknowledged.

TABLE OF CONTENTS

LIST OF SYMBOLS

A, B, C - see (1.17)

A_n, B_n - see (2.20)

a_s - speed of sound in panel material, see (3.22)

a_∞ - speed of sound in ambient air

b - dimensional panel width

C_n - see (1.18)

$D(k,s)$ - flutter determinant, see (2.10) and (2.13) or (2.25) and (2.26)

$\bar{D}^{\pm}(p)$ - see (2.14)

D_x, D_{x_0} - flexural rigidity, see (1.5)

E_x, E_y - Young's modulii

F_n - see (2.20)

$F(x)$ - characteristic function, see (2.7) and (2.24)

$f(x)$ - chordwise flutter mode shape

$G_n(x)$ - see (2.20)

G_{xy} - shear modulus

g - structural damping

$g(p)$ - see (2.15)

$g(y)$ - spanwise mode shape, see Appendix A

h - dimensional panel thickness

$h(p)$ - see (2.15)

J_0 - Bessel function

K - supersonic reduced frequency kM/β^2

K_e - elastic foundation parameter

k - reduced frequencies $\omega b/U$

$\ell(p)$ - see (2.15)

LIST OF SYMBOLS (Cont.)

M - Mach number

N_{x_1}, N_{y_1} - average nonlinear membrane stresses

N_x, N_y, N_{xy} - total membrane stresses

$N_{x_0}, N_{y_0}, N_{xy_0}$ - applied membrane stresses

$\hat{N}_{x_1}, \hat{N}_{y_1}, \hat{N}_{xy}$ - average membrane stresses

$\bar{n}$ - number of half waves per panel width in the spanwise mode shape

$P(x)$ - dimensionless aerodynamic pressure

p - aerodynamic pressure in Section I (lb/ft^2) Laplace transform variable otherwise

p_A, p_B - branch points, see Fig. 2a

p_n - ten characteristic roots

R - see (1.17) and Appendix C

r_{x_0}, r_{y_0} - applied membrane stress parameters, see (1.17)

r_{x_1}, r_{y_1} - nonlinear membrane stress parameters, see (1.17)

$r_x, r_y = r_{x_0} + r_{x_1}, r_{y_0} + r_{y_1}$, respectively

S, S_0 - dynamic pressure parameter, see (1.17) and Appendix C

s - length-to-width ratio

s_x, s_y - dimensionless stress parameters, see (1.21)

t - dimensionless time

U - free stream velocity

u, v - midplane deflections

W - amplitude of motion in panel thicknesses

$w(x,y,z)$ - panel deflection

x, y, z - coordinate system, see Fig. 1, p. 5

LIST OF SYMBOLS (Cont.)

β	- $\sqrt{M^2 - 1}$
β_n	- parameter in spanwise mode shape
Γ	- constant, see (2.4)
γ	- viscous damping parameter
$\Delta(p)$	- characteristic polynomial, see (2.16)
ϵ_c, ϵ_p	- stringer restraint parameters
η	- material altitude parameter, see Appendix C
λ	- wave length in traveling-wave solution
μ	- mass ratio parameter, see Appendix C
$\mu_{s.w.}$	- standing-wave flutter μ for $s \to \infty$
$\mu_{t.w.}$	- traveling-wave flutter μ for $s \to \infty$
ν_x, ν_y	- Poisson ratios
ρ_s	- mass density of panel material
ρ_∞	- free stream density
σ_x, σ_y	- total stress
τ	- thickness-to-width ratio (h/b)
ϕ	- velocity potential
Ω_{xy}, Ω_{yy}	- orthotropic constants
ω	- frequency

See Appendix C for further discussion and use of some of the principal dimensionless parameters.

LIST OF FIGURES

INTRODUCTION

The problem of panel flutter has been actively studied theoretically and experimentally by many authors over the past two decades. For a complete bibliography of work up to 1968, one should consult Volume II of the extensive design criteria effort of C. E. Lemley (Ref. 1). A more recent review article by Dowell (Ref. 2) covers the period after 1968 to the present time.

Many formulations of the panel flutter problem have appeared in the literature with varying levels of complexity. Most of these studies have dwelled on the linear stability problem. Inviscid aerodynamic theory was used, either the exact inviscid theory following Garrick and Rubinow (Ref. 3) or the static and quasi-steady approximation thereof. Only in recent years has the importance of the boundary layer been realized and investigated in a rational manner. The most definitive work in this area is the experimental effort of Muhlstein, et al.(Refs. 4,5). A completely satisfactory theory is still lacking but the recent work of Dowell (Ref. 6) is a step toward this goal.

The need for a nonlinear formulation and analysis of panel flutter became evident when it was realized that panel flutter is not always destructive. If the stress level during the post-flutter limit cycle oscillation is sufficiently low, many cycles of stress reversal can be tolerated without failure. In one-shot missile applications, it may be too severe a weight penalty to demand complete absence of panel flutter. The problem of estimating the post-flutter stress level then comes to the fore as a significant design problem.

The problem of nonlinear flutter of flat panels was analyzed by Bolotin (Ref. 7) who used the Galerkin method in the spatial variables and the method of Krylov and Bogoliubov in the time variable. Olson and Fung (Ref. 8) applied the same method to the cylindrical shell. The assumptions of weak nonlinearity, small damping and weakly-coupled modes are difficult to justify,

however, in the application of this method to panel flutter. To avoid these limitations, Dowell (Refs. 9,10) has attacked the problem with the Galerkin method in the spatial variable and direct numerical integration of the nonlinear ordinary differential equations in time. This is the most complete attack on the problem to date. The principal disadvantage of Dowell's approach is the amount of computer time required. A further work of interest in this area is due to Eastep (Ref. 11) who considers the coupled response to a turbulent boundary layer and the nonlinear limit cycle motion.

Another approach that seeks to obtain an estimate of the stresses in the panel is due to Zeydel (Ref. 12). The philosophy underlying his approach is that a detailed description of the stress distribution in the panel is not really needed, but rather an estimate of the peak stress. The further supposition is made that this estimate can be obtained by averaging the nonlinear membrane stresses to obtain an equivalent linear problem. The method proposed by Zeydel is presented in detail in the present report, together with some example numerical calculations.

Different methods have been employed to attack various formulations of the linear flutter problem. The most common approach is the Galerkin method, in particular, when the full linearized aerodynamic theory is incorporated. Exact methods have been used successfully when either the static or quasi-steady aerodynamic theory is used; e.g., see Refs. 13, 14, 15. The Galerkin method is a very powerful tool for solving the exact problem when the length-to-width ratio is small, of order unity. For such geometry, the flutter mode shape can be approximated closely with only a few assumed modes so that the resulting flutter matrix is of tractable size. However, when the length-to-width ratio becomes large, the number of half waves in the chordwise flutter mode becomes large and also the mode shape has an exponential growth near the trailing edge. To resolve this type of flutter mode into Fourier components, one must use a large number of assumed

modes and, consequently, must be able to handle a very large flutter matrix to obtain convergence. The result is that the computational effort grows out of all proportion to the magnitude of the problem.

In Refs. 16 and 17, a new method for solving an exact formulation of the problem was introduced. The problem treated is that of an infinite spanwise array of identical panels. Exact inviscid aerodynamic theory is employed. The technique is to reduce the full problem to an ordinary differential equation in the streamwise variable. The latter problem is solved by Laplace transforms in a way suggested by Goland and Luke (Ref. 18) for investigating the problem of membrane flutter. The convergence difficulties associated with the Galerkin method are avoided, in that the mode shape and its derivatives are obtained quite naturally in the process of solution. The present effort is an extension of the work initiated by the late Dr. E. F. E. Zeydel in Refs. 16 and 17 and, in fact, supercedes the work in Ref. 17.

We remark, in conclusion, that many of the results presented herein may appear to the experienced worker in the field to be a restatement of known facts accumulated over two decades of research on the problem. This is in part true. The only justification offered is that most of the accumulated knowledge on the subject that the author is aware of can be derived and explained in a unified way at a very fundamental level with the exact method used herein. If this unification of our knowledge results in even a small advancement of the state of the art, then the effort has been worthwhile.

I. PROBLEM FORMULATION

A. Equations of Motion and Boundary Conditions

Referring to Fig. 1 we consider an infinite spanwise array of identical flat rectangular panels of unit width and length s in a supersonic mainstream of velocity U. A dimensional panel width b will be carried in the key dimensionless parameters. The panel material is assumed to be homogeneous and of uniform thickness τ, but may be orthotropic. Also, we include the effects of viscous damping, structural damping and an elastic foundation in the analysis.

The nonlinear equation of motion and stress definitions for the panel array is (Ref. 7):

$$\frac{D_x}{b^3}\nabla^4 w - \frac{N_x}{b}\frac{\partial^2 w}{\partial x^2} - \frac{N_y}{b}\frac{\partial^2 w}{\partial y^2} - 2\frac{N_{xy}}{b}\frac{\partial^2 w}{\partial x \partial y} + K_e b w + \gamma U \frac{\partial w}{\partial t} + \rho_s \tau U^2 \frac{\partial^2 w}{\partial t^2} = p \tag{1.1}$$

where

$$\nabla^4 = \frac{\partial^4}{\partial x^4} + 2\Omega_{xy}\frac{\partial^4}{\partial x^2 \partial y^2} + \Omega_{yy}\frac{\partial^4}{\partial y^4} \tag{1.2}$$

$$N_x = N_{x_o} + \frac{(1+ig)E_x b}{1-\nu_x\nu_y}\left[\frac{\partial u}{\partial x} + \frac{1}{2}\left(\frac{\partial w}{\partial x}\right)^2 + \nu_y\left\{\frac{\partial v}{\partial y} + \frac{1}{2}\left(\frac{\partial w}{\partial y}\right)^2\right\}\right]$$

$$N_y = N_{y_o} + \frac{(1+ig)E_y b}{1-\nu_x\nu_y}\left[\frac{\partial v}{\partial y} + \frac{1}{2}\left(\frac{\partial w}{\partial y}\right)^2 + \nu_x\left\{\frac{\partial u}{\partial x} + \frac{1}{2}\left(\frac{\partial w}{\partial x}\right)^2\right\}\right]$$

$$N_{xy} = N_{xy_o} + bG_{xy}\left(\frac{\partial v}{\partial x} + \frac{\partial u}{\partial y}\right) \tag{1.3}$$

$$\sigma_x = \frac{N_x}{h} - \frac{\tau}{2}\frac{E_x}{1-\nu_x\nu_y}\left(\frac{\partial^2 w}{\partial x^2} + \nu_x\frac{\partial^2 w}{\partial y^2}\right)$$

$$\sigma_y = \frac{N_y}{h} - \frac{\tau}{2}\frac{E_y}{1-\nu_x\nu_y}\left(\frac{\partial^2 w}{\partial y^2} + \nu_y\frac{\partial^2 w}{\partial x^2}\right) \tag{1.4}$$

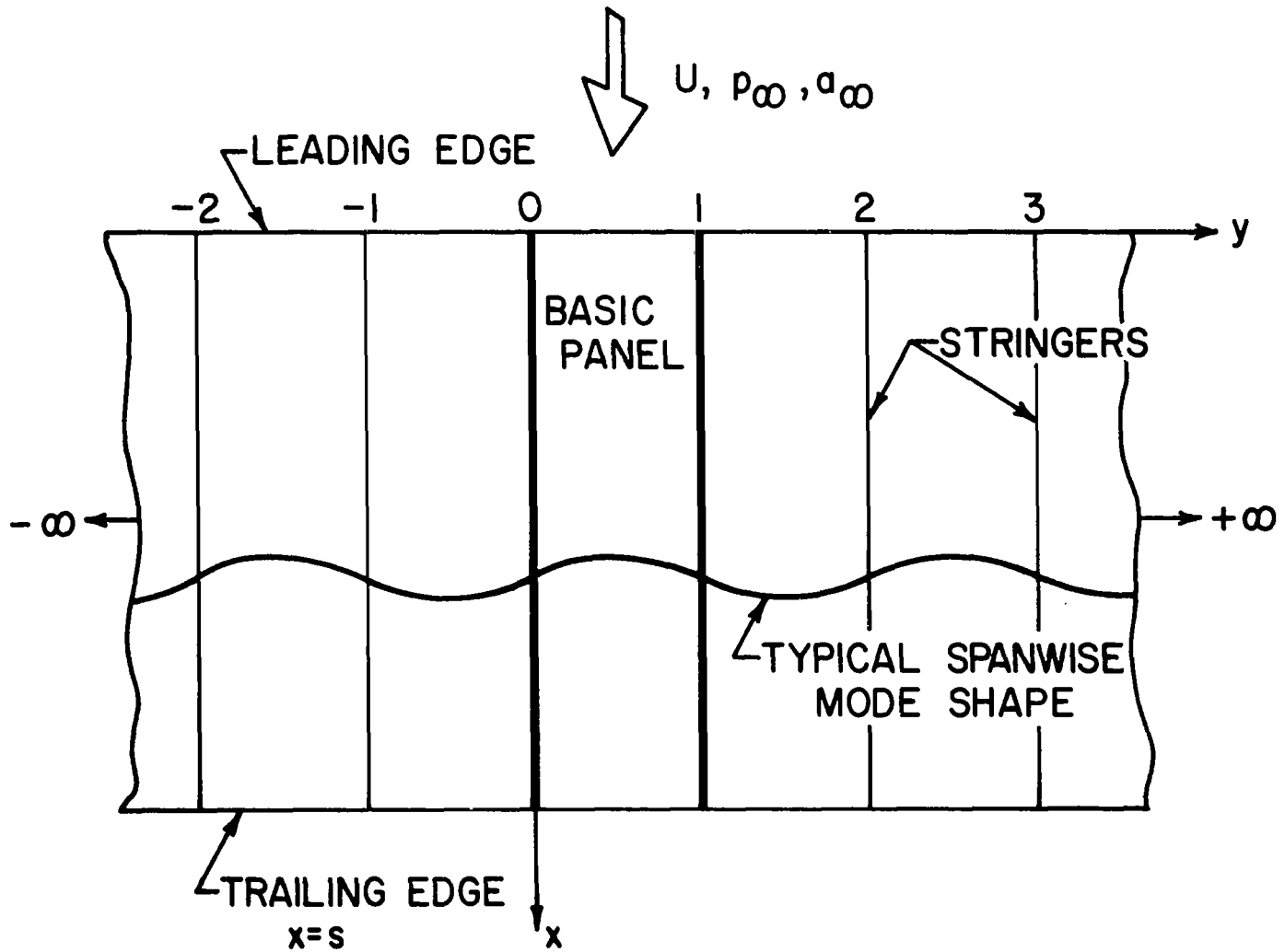

FIGURE 1. SPANWISE ARRAY OF PANELS

and

$$\Omega_{xy} = \frac{D_{xy}}{D_x} \quad , \quad \Omega_{yy} = \frac{D_y}{D_x}$$

$$D_x = (1 + ig)D_{x_o} \quad , \quad D_{x_o} = \frac{E_x h^3}{12(1 - \nu_x \nu_y)} \qquad (1.5)$$

In (1.1) the unit of time is b/U .

Structural damping is incorporated in two places in the foregoing equations. First in the complex bending modulus D_x and second in the nonlinear stress terms (1.3). We point out that structural damping is not included in the applied membrane stresses N_{x_o} , N_{y_o} , N_{xy_o} . The elastic foundation and viscous damping are included via the terms $K_e b w$ and $\gamma U b \frac{\partial w}{\partial t}$ in (1.1). Orthotropicity is incorporated through the different elastic modulii in the x and y directions. The total stresses in the panel are given by (1.4) and are the sum of three parts: (1) the applied membrane stresses, (2) the nonlinear membrane stresses that develop with large amplitude motion and (3) the bending stresses.

The boundary conditions needed to complete the formulation of the problem are the following. The midplane displacements u,v and normal deflection ω are assumed to be zero on the leading and trailing edge and on each of the stringers. The leading and trailing edges may be pinned or clamped and the longitudinal stringers may offer a partial torsional restraint into the panel. Thus, we have

$$u = v = w = 0 \quad \text{when} \quad x = 0,s$$
$$\text{or} \quad y = n$$

Leading and trailing edges

$$\frac{\partial^2 w}{\partial x^2} = 0 \quad , \quad x = 0,s \quad \text{pinned}$$

$$\frac{\partial w}{\partial x} = 0 \quad , \quad x = 0,s \quad \text{clamped}$$

Stringers

$$\frac{\epsilon_p}{2}\left(\left.\frac{\partial^2 w}{\partial y^2}\right|_{y=n^+} - \left.\frac{\partial^2 w}{\partial y^2}\right|_{y=n^-}\right) = \epsilon_c \left.\frac{\partial w}{\partial y}\right|_{y=n}$$

$$\text{for} \quad n = \ldots -2, -1, 0, 1, 2 \ldots \tag{1.6}$$

where ϵ_c and ϵ_p vary between zero and unity and give the degree of restraint of the stringers; e.g., if $\epsilon_c = 0$ and $\epsilon_p = 1$ the stringer has no restraint and if $\epsilon_c = 1$, $\epsilon_p = 0$, it is completely restrained.

B. Stress Estimation Procedure

We note that our basic set of equations and boundary conditions is incomplete. Additional equilibrium equations and compatibility equations for the midplane stresses are needed before a complete solution can be attempted. The omission is deliberate, however, since we propose to handle the nonlinear membrane stresses by an averaging procedure that does not require explicit use of these equilibrium equations.

The averaging technique for estimating the stresses during panel flutter was suggested by Zeydel (Ref. 12) and goes as follows. Flutter is supposed to occur initially in the linear regime. After the initial onset of flutter the amplitude grows to some value that is limited by the nonlinear membrane stresses. The key assumption is that the nonlinear limit cycle motion is approximately governed by an equation of the form (1.1), but with the membrane stresses replaced by appropriate average values. The main consequence of the averaging is that the problem becomes linear. Here we average N_x, N_y and N_{xy} over the area of a single panel and one period of oscillation. We define

$$\hat{N} = \frac{1}{s \cdot T}\int_0^s dx \int_0^l dy \int_0^T dt \cdot N \tag{1.7}$$

where N is any stress component. Substituting N_x, N_y and N_{xy} in turn into (1.7) and using the boundary conditions on u, v we get

$$\hat{N}_x = N_{x_o} + (1 + ig)\, N_{x_1}$$

$$\hat{N}_y = N_{y_o} + (1 + ig)\, N_{y_1}$$

$$\hat{N}_{xy} = N_{xy_o} \tag{1.8}$$

where

$$N_{x_1} = \frac{E_x b}{2(1 - \nu_x \nu_y)} \cdot \frac{1}{sT} \int_0^s dx \int_0^1 dy \int_0^T dt \left(w_x^{\,2} + \nu_y w_y^{\,2} \right)$$

$$N_{y_1} = \frac{E_y b}{2(1 - \nu_x \nu_y)} \cdot \frac{1}{sT} \int_0^s dx \int_0^1 dy \int_0^T dt \left(w_y^{\,2} + \nu_x w_x^{\,2} \right) \tag{1.9}$$

The procedure for calculating flutter and estimating the limit cycle stresses is thus reduced to the following steps:

1. Replace N_x, N_y, N_{xy} by their averages $\hat{N}_x$, $\hat{N}_y$, $\hat{N}_{xy}$ in (1.1) and in (1.4).
2. Assume values of N_{x_1} and N_{y_1} and compute a flutter point and mode shape.
3. Substitute the mode shape into either of (1.9) to determine the unknown amplitude.
4. Estimate the stress by direct calculation with (1.4).

C. Aerodynamic Forces

In the present study we use exact inviscid linearized aerodynamic forces, except where comparisons are made with static theory. If ϕ is the perturbation velocity potential, then the problem we must solve to obtain the pressure p is the following:

$$\beta^2 \frac{\partial^2\phi}{\partial x^2} - \frac{\partial^2\phi}{\partial y^2} - \frac{\partial^2\phi}{\partial z^2} + 2M^2 \frac{\partial^2\phi}{\partial x \partial t} + M^2 \frac{\partial^2\phi}{\partial t^2} = 0$$

$$\beta^2 = M^2 - 1$$

$$\left.\frac{\partial\phi}{\partial z}\right|_{z=o} = \frac{\partial w}{\partial x} + \frac{\partial w}{\partial t}$$

Outgoing waves at infinity (1.10)

$$p = - \rho_\infty U^2 \left(\frac{\partial\phi}{\partial x} + \frac{\partial\phi}{\partial t}\right)_{z=0} \tag{1.11}$$

The solution of the aerodynamic problem is well known for the case of simple harmonic motion and a panel array (see, e.g., Ref. 17). Rather than adopt the known explicit solution for p at this point, however, we shall leave the problem in the form of (1.10) and (1.11). The reason is that we want to illustrate how the flutter problem can be formulated and solved by Laplace transforms with only a knowledge of the transform of p.

D. Reduction of the Flutter Problem to an Ordinary Differential Equation

To solve the flutter problem by the Zeydel method, which uses the Laplace transform, we first reduce the problem to the solution of an ordinary differential equation in x. We assume the deflection and velocity potential to be of the form

$$w = \tau W g(y)\ \mathrm{Re}\left\{f(x)e^{ikt}\right\}$$
$$\phi = \tau W g(y)\ \mathrm{Re}\left\{\phi(x,z)e^{ikt}\right\} \tag{1.12}$$

where

$$k = \frac{\omega b}{U} \quad \text{reduced frequency based on panel width}$$

$$g(y) = \quad \text{spanwise mode shape}$$

$$W = \quad \text{amplitude in panel thicknesses} \qquad (1.13)$$

We choose the spanwise mode shape a priori and carry out a single mode Galerkin analysis in the spanwise direction. The mode shape we choose is the beam vibration mode that satisfies the boundary condition at the stringers (see (1.6)). Thus $g(y)$ is a solution of the following problem:

$$\frac{d^4 g}{dy^4} - \beta_{\bar{n}}^4 g = 0 \qquad 0 < y < 1$$

$$g(0) = g(1) = 0$$

$$\epsilon_c g'(0) - \epsilon_p g''(0) = 0$$

$$\epsilon_c g'(1) + \epsilon_p g''(1) = 0 \qquad (1.14)$$

and

$$g(y + n) = - (- 1)^{n+\bar{n}} g(y) \qquad n = \ldots -2, -1, 0, 1, 2 \ldots$$

$$0 < y < 1 \qquad (1.15)$$

where $\bar{n}$ is the spanwise mode number or number of half waves in a single panel width. The periodic extension of $g(y)$, (1.15), is such that the panels are alternately in and out of phase (see Fig. 1). The solution of (1.14) for arbitrary stringer restraints ϵ_p and ϵ_c is given in Appendix A, together with appropriate integrals of $g(y)$ that are needed in the subsequent discussion.

Next we substitute (1.12) into the equations of motion and aerodynamic problem, multiply by $g(y)$ and integrate over the infinite span of the panel to obtain the following formulation of the flutter and stress estimation problem:

Reduced Equation of Motion

$$\frac{d^4f}{dx^4} - A\frac{d^2f}{dx^2} + C\frac{df}{dx} + Bf + SP(x) = 0 \qquad (1.16)$$

where

$$A = 2C_2\Omega_{xy} + \frac{r_{x_o}}{1 + ig} + r_{x_1}$$

$$B = \beta_n^4\,\Omega_{yy} + C_2 r_{y_1} + \frac{C_2 r_{y_o} + b^3(K_e b + i\gamma Uk)/D_{x_o} - Rk^2}{1 + ig}$$

$$C = \frac{2C_1 r_{xy_o}}{1 + ig}$$

$$S = \frac{S_o}{1 + ig}$$

$$R = \frac{\rho_s h b^2 U^2}{D_{x_o}} \quad , \quad S_o = \frac{\rho_\infty U^2 b^3}{D_{x_o}}$$

$$r_{x_o} = \frac{N_{x_o} b^2}{D_{x_o}} \quad , \quad r_{y_o} = \frac{N_{y_o} b^2}{D_{x_o}}$$

$$r_{x_1} = \frac{N_{x_1} b^2}{D_{x_o}} \quad , \quad r_{y_1} = \frac{N_{y_1} b^2}{D_{x_o}} \qquad (1.17)$$

and

$$C_n = -\int_0^1 \frac{d^n g(y)}{dy^n}\, g(y)\, dy \qquad \text{(See Appendix A)} \qquad (1.18)$$

Boundary Conditions

$$f(0) = f(s) = 0$$

$$f'(0) = f'(s) = 0 \qquad \text{clamped ends}$$

$$f''(0) = f''(s) = 0 \qquad \text{pinned ends} \qquad (1.19)$$

Aerodynamic Problem

$$\beta^2 \frac{\partial^2 \phi}{\partial x^2} - \frac{\partial^2 \phi}{\partial z^2} + 2ikM^2 \frac{\partial \phi}{\partial x} + \left(C_2 - k^2 M^2\right) \phi = 0$$

$$\left.\frac{\partial \phi}{\partial z}\right|_{z=0} = \frac{\partial f}{\partial x} + ikf$$

Outgoing waves at infinity

$$P(x) = -\left(\frac{\partial \phi}{\partial x} + ik\phi\right)_{z=0} \qquad (1.20)$$

Mode Shape and Maximum Stress Estimation

$$w = \tau W g(y)\ \mathrm{Re}\left\{f(x)e^{ikt}\right\}$$

$$W = \left[\frac{r_{x_1} \tau s}{3\int_0^s \left(|f'(x)|^2 - C_2 \nu_y |f(x)|^2\right) dx}\right]^{1/2}$$

$$\frac{r_{y_1}}{r_{x_1}} = \Omega_{yy} \frac{\int_0^s \left(\nu_x |f'|^2 - C_2 |f|^2\right) dx}{\int_0^s \left(|f'|^2 - C_2 \nu_y |f|^2\right) dx}$$

$$s_x = \frac{12\sigma_{x_{max}} (1 - \nu_x \nu_y)}{E_x \tau^2} = r_{x_o} + r_{x_1}$$

$$+ 6 \cdot W \cdot \underset{\substack{0<y<1 \\ 0<x<s \\ 0<t<\frac{\pi}{k}}}{\mathrm{Max}} \left\{g(y)\mathrm{Re}(f'' e^{ikt}) + \nu_x g''(y)\mathrm{Re}(f e^{ikt})\right\}$$

$$s_y = \frac{12\sigma_{y_{max}}(1 - \nu_x\nu_y)}{E_x\tau^2} = r_{y_o} + r_{y_1}$$

$$+ 6 \cdot W \cdot \underset{\substack{0<y<1 \\ 0<x<s \\ 0<t<\frac{\pi}{k}}}{\text{Max}} \left\{ g''(y)\text{Re}(fe^{ikt}) + \nu_y g(y)\text{Re}(f\tilde{}e^{ikt}) \right\} \tag{1.21}$$

We remark that the third formula of Eq. (1.21) is a compatibility condition on the initial assumption for r_{y_1} and r_{x_1}.

Remarks on Midplane Shear Stress

The term $C\frac{df}{dx}$ in (1.16) contains the effect of an applied midplane shear stress in the array of panels. It is most interesting since it is exactly the same form as aerodynamic stiffness. Hence, by applying the shear stress of appropriate sign, flutter could conceivably be induced or eliminated.

Although the possibility of a flutter control mechanism by applied shear is interesting, a closer inspection of the problem reveals that it is not possible within the framework of the present theory. The integral C_1 that appears in the definition of the shear term is identically zero (see Appendix A). In the subsequent discussion we shall omit the shear term.

II. EXACT SOLUTION

A. The Zeydel Method

Here we show in detail how the flutter problem is solved by the Zeydel method. The method was developed by Zeydel (Refs. 16, 17) to circumvent some of the difficulties inherent in the Ritz-Galerkin procedure when the panel length-to-width ratio becomes large. It yields directly the flutter boundary and mode shapes that are essential for stress estimation, without reference to assumed modes. Some of the subsequent detail was given initially in Ref. 17 and is included here for completeness.

Introduce the Laplace transform in the chordwise direction:

$$\bar{f}(p) = \int_0^\infty e^{-px} f(x)\, dx$$

$$f(x) = \frac{1}{2\pi i} \int_{\gamma-i\infty}^{\gamma+i\infty} e^{px} \bar{f}(p)\, dp \qquad (2.1)$$

where γ is to the right of all singularities of $\bar{f}(p)$. Now take the Laplace transform of (1.16) to obtain

$$(p^4 - Ap^2 + B)\,\bar{f} + S\bar{P}(p) = (p^2 - A)\, f_o' + pf_o'' + f_o''' \qquad (2.2)$$

where f_o', f_o'', f_o''' are the derivatives of $f(x)$ at the leading edge. Note that the boundary condition $f_o = 0$ has been used and that either f_o' or f_o''' is zero when the distinction of pinned or clamped leading edge is made. For the moment we shall carry both terms in (2.2).

The Laplace transform of the pressure $\bar{P}(p)$ is evaluated as follows. We take the Laplace transform of the complete aerodynamic problem (1.20). Thus

$$\frac{d^2\bar{\phi}}{dz^2} - \left(\beta^2 p^2 + 2ikM^2 p - k^2M^2 + C_2\right)\bar{\phi} = 0$$

$$\left.\frac{d\bar{\phi}}{dz}\right|_{z=o} = (p + ik)\bar{f}$$

$$\bar{P}(p) = (p + ik)\bar{\phi}\big|_{z=o} \qquad (2.3)$$

After solving for $\bar{\phi}$ we obtain

$$\bar{P}(p) = \frac{(p + ik)^2}{\beta\left[(p + iKM)^2 + \Gamma^2\right]^{\frac{1}{2}}} \bar{f}(p)$$

$$K = \frac{kM}{\beta^2} \quad , \quad \Gamma = \left(K^2 + \frac{C_2}{\beta^2}\right)^{\frac{1}{2}} \tag{2.4}$$

We point out that the actual pressure mode shape $P(x)$ is not needed to solve the problem with the Zeydel method.

Now substitute (2.4) into (2.2) and solve for $\bar{f}(p)$. We get

$$\bar{f}(p) = \frac{(p^2 - A)f_o' + pf_o'' + f_o'''}{\bar{D}^+(p)} \tag{2.5}$$

where

$$\bar{D}^+(p) = p^4 - Ap^2 + B + \frac{S}{\beta} \frac{(p + ik)^2}{\left[(p + iKM)^2 + \Gamma^2\right]^{\frac{1}{2}}} \tag{2.6}$$

Define the function

$$F(x) = \frac{1}{2\pi i} \int_{\gamma - i\infty}^{\gamma + i\infty} \frac{e^{px}}{\bar{D}^+(p)} \, dp \tag{2.7}$$

so that the inverse transform of (2.5) can be expressed in the form

$$f(x) = (F''(x) - AF(x))f_o' + F(x)f_o''' \qquad \text{pinned}$$

$$= F'(x)f_o'' + F(x)f_o''' \qquad \text{clamped} \tag{2.8}$$

Now apply the boundary conditions at the trailing edge ($x = s$) . The results can be summarized as follows:

For Pinned Edges

$$\begin{bmatrix} F''(s) - AF(s) & F(s) \\ F''''(s) - AF''(s) & F''(s) \end{bmatrix} \begin{pmatrix} f_o' \\ f_o''' \end{pmatrix} = 0 \qquad (2.9)$$

For fixed s this system is interpreted as a pair of equations for f_o' and f_o'''. To obtain a nontrivial solution it is necessary that the determinant of the coefficient matrix vanish, or

$$D = F(s)F''''(s) - F''^2(s) = 0 \qquad (2.10)$$

The last result is the flutter condition within the present framework and must be solved to obtain the flutter eigenvalues. For each eigenvalue, we then solve (2.9) for the ratio f_o'/f_o''' and substitute into (2.8) to obtain the flutter mode shape,

$$f(x) = \frac{F''(x)}{F''(s)} - \frac{F(x)}{F(s)} \qquad (2.11)$$

For Clamped Edges

The argument proceeds in exactly the same way for clamped edges. The counterpart of the system (2.9) is

$$\begin{bmatrix} F'(s) & F(s) \\ F''(s) & F'(s) \end{bmatrix} \begin{pmatrix} f_o'' \\ f_o''' \end{pmatrix} = 0 \qquad (2.12)$$

The flutter condition and mode shape are given respectively by

$$D = F(s)F''(s) - F'^2(s) = 0$$

$$f(x) = \frac{F'(x)}{F'(s)} - \frac{F(x)}{F(s)} \qquad (2.13)$$

The procedure for calculating flutter boundaries and mode shapes with the Zeydel method is the following:

1. Fix all but two of the parameters entering into the problem. We shall see that the reduced frequency k and the length-to-width ratio s are convenient free parameters;
2. Search the plane of free parameters for zeros (flutter points) of the complex determinant $D(k,s)$;
3. Evaluate the normalized mode shape by direct calculation at the flutter points.
4. Use the flutter point and normalized mode shape to estimate the maximum stress with (1.21).

B. Evaluation of the Characteristic Function $F(x)$

The success of the Zeydel method depends upon the evaluation of the characteristic function $F(x)$ and its derivatives (see (2.7)). Here we show a procedure that has been used successfully.

We first extend the definition of $\bar{D}^+(p)$ such that

$$\bar{D}^{\pm}(p) = g(p) \pm \frac{\ell(p)}{h^{\frac{1}{2}}(p)} \tag{2.14}$$

where

$$g(p) = p^4 - Ap^2 + B$$

$$\ell(p) = \frac{S}{\beta}(p + ik)^2$$

$$h(p) = (p + iKM)^2 + r^2 \tag{2.15}$$

Define the quantity

$$\Delta(p) = h(p)\,\bar{D}^+(p)\bar{D}^-(p) \tag{2.16}$$

and observe that it is a tenth degree polynomial in p with roots p_n, $n = 1,2,\ldots,10$. These roots are, in general, distinct so that

$$\frac{1}{\Delta(p)} = \sum_{n=1}^{10} \frac{1}{\Delta'(p_n)(p - p_n)}$$

$$\Delta'(p) = \frac{d}{dp}\Delta(p) \tag{2.17}$$

Now multiply the numerator and denominator in (2.7) by $h(p)\bar{D}^{-}(p)$ and write $F(x)$ in the form

$$F(x) = \frac{1}{2\pi i} \int_{\gamma-i\infty}^{\gamma+i\infty} \frac{e^{px} h(p) g(p)}{\Delta(p)}\, dp$$

$$- \frac{1}{2\pi i} \int_{\gamma-i\infty}^{\gamma+i\infty} e^{px}\, \frac{h(p)\ell(p)}{\Delta(p)} \cdot \frac{dp}{h^{1/2}(p)} \tag{2.18}$$

Substitute (2.17) into (2.18) and evaluate each term separately. The result can be expressed concisely in the following form:

$$F(x) = \sum_{n=1}^{10} F_n(x) \tag{2.19}$$

where

$$F_n(x) = e^{p_n x}(A_n - B_n G_n(x))$$

$$G_n(x) = \int_0^x e^{-(p_n + iKM)\xi}\, J_o(\Gamma\xi)\, d\xi$$

$$A_n = \frac{h(p_n) g(p_n)}{\Delta'(p_n)} \quad , \quad B_n = \frac{h(p_n)\ell(p_n)}{\Delta'(p_n)} \tag{2.20}$$

and $J_o(z)$ is the Bessel function of zero order.

The foregoing procedure can be used to evaluate $F(x)$ numerically (see Appendix B). It remains to be shown how the derivatives of $F(x)$ can be evaluated efficiently and accurately.

The scheme is based on the following result:

$$\int_C \frac{p^m}{\Delta(p)}\,dp = 0 \quad , \; m = 1,2,\ldots,8 \tag{2.21}$$

where C is any closed curve that contains all of the poles of the integrand. The result is easily proved by reversing the path of integration and noting that there is no residue at infinity. It follows at once from (2.17) and (2.21) that

$$\sum_{n=1}^{10} \frac{p_n^m}{\Delta'(p_n)} = 0 \tag{2.22}$$

and so

$$\sum_{n=1}^{10} A_n p_n^m = 0 \quad , \; m = 0,1,2$$

$$\sum_{n=1}^{10} B_n p_n^m = 0 \quad , \; m = 0,1,2,3,4 \tag{2.23}$$

With the foregoing results it is readily verified that $F(x)$ and its first four derivatives can be expressed in the convenient form

$$F^{(m)}(x) = \sum_{n=1}^{10} p_n^m F_n(x) \quad , \quad m = 0,1,2,3,4 \tag{2.24}$$

Finally, we substitute the last result into the flutter condition and mode shape (2.10), (2.11) and (2.13) to obtain:

For Pinned Edges

$$D(k,s) = \sum_{n=1}^{9} \sum_{m=n+1}^{10} F_n(s)F_m(s)\left(p_n^2 - p_m^2\right)^2 = 0$$

$$f^{(m)}(x) = \frac{\sum_{n=1}^{10} p_n^{m+2} F_n(x)}{\sum_{n=1}^{10} p_n^2 F_n(s)} - \frac{\sum_{n=1}^{10} p_n^m F_n(x)}{\sum_{n=1}^{10} F_n(s)} \quad , \quad m = 0,1,2 \tag{2.25}$$

For Clamped Edges

$$D(k,s) = \sum_{n=1}^{9} \sum_{m=n+1}^{10} F_n(s)F_m(s)(p_n - p_m)^2 = 0$$

$$f^{(m)}(x) = \frac{\sum_{n=1}^{10} p_n^{m+1} F_n(x)}{\sum_{n=1}^{10} \rho_n F_n(s)} - \frac{\sum_{n=1}^{10} p_n^{m} F_n(x)}{\sum_{n=1}^{10} F_n(s)}, \quad m = 0,1,2 \qquad (2.26)$$

The entire problem of evaluating flutter boundaries, mode shapes and their derivatives has been reduced to the evaluation of ten functions $F_n(x)$ that correspond to the ten roots of the characteristic polynomial. A detailed numerical procedure is given in Appendix B.

C. Discussion of the Root Plane

The typical locations of the ten roots of the characteristic polynomial are shown in the complex p-plane in Fig. 2, together with the two branch points, $p_{A,B} = -iKM \pm i\Gamma$, of the transformed aerodynamic pressure (see (2.4)). Here we discuss the physical significance of these singularities and also how they move in the complex p-plane with a change of reduced frequency, mass ratio parameter and other parameters. We shall see that the very essence of panel flutter is contained in the singularities of the root plane.

Some general properties

If one introduces the transformation $p = i\lambda$ in $\Delta(p)$, (2.16), the coefficients of the resulting polynomial in λ are real providing that structural and viscous damping are zero. Even for small values of damping, the λ roots are nearly conjugate pairs. This means that root pairs in the p-plane are nearly conjugate about the imaginary axis. From Fig. 2 we see

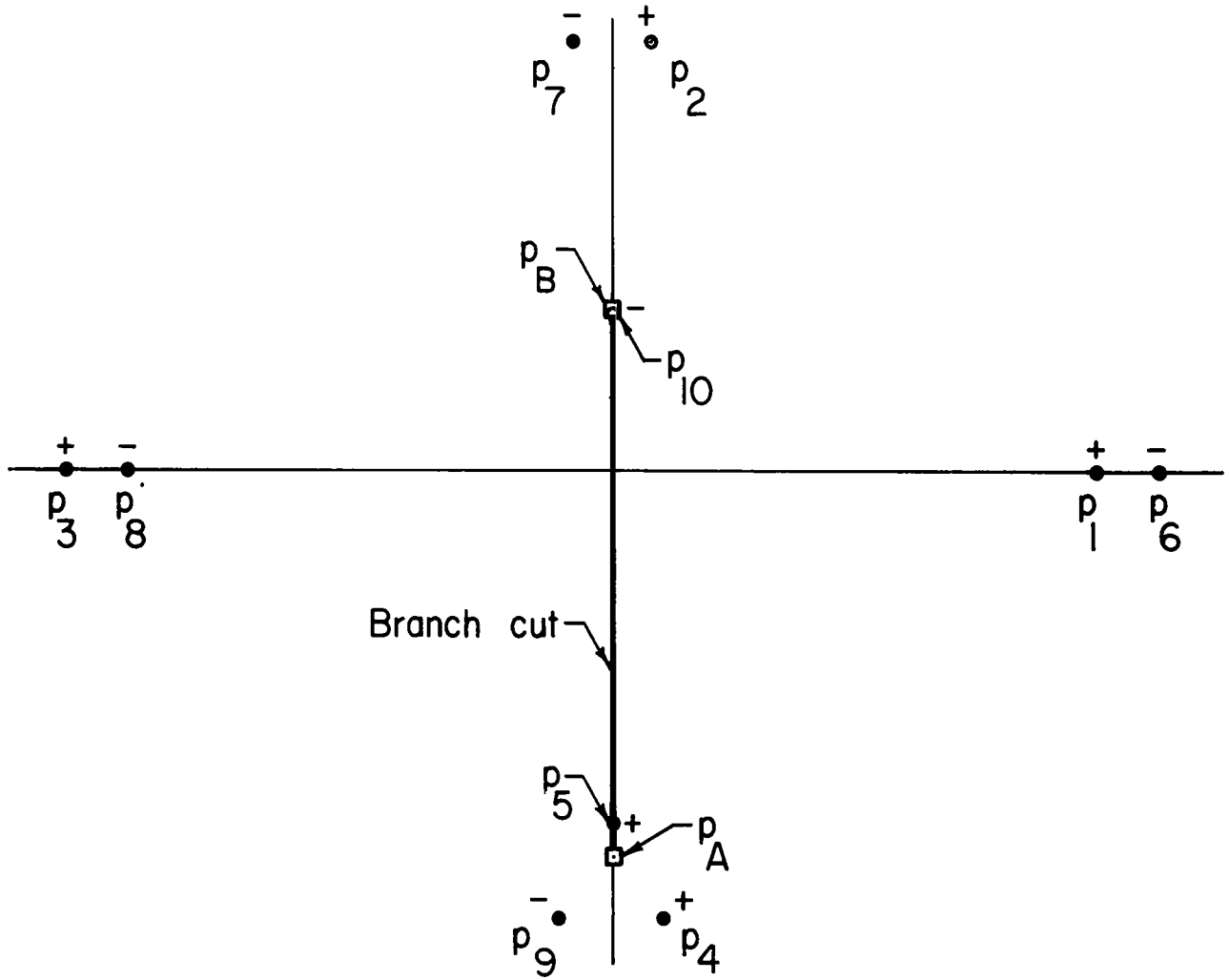

FIGURE 2a. TYPICAL ROOT LOCATION IN THE COMPLEX p-plane; $\mu = 58$, $\eta = 1.35$, $M = 1.35$, $g = 0.01$, $k = 0.65$.

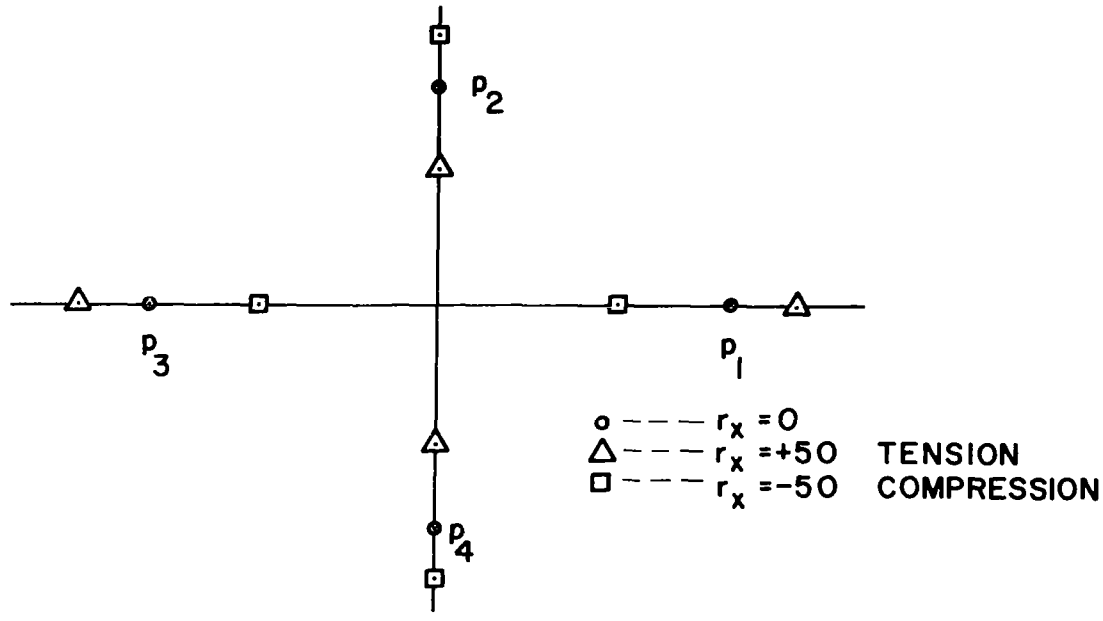

FIGURE 2b. TYPICAL ROOT LOCATION WITHOUT AERODYNAMIC FORCES AND SHIFT DUE TO MEMBRANE FORCES; R = 4250, k = 0.65, g = 0.

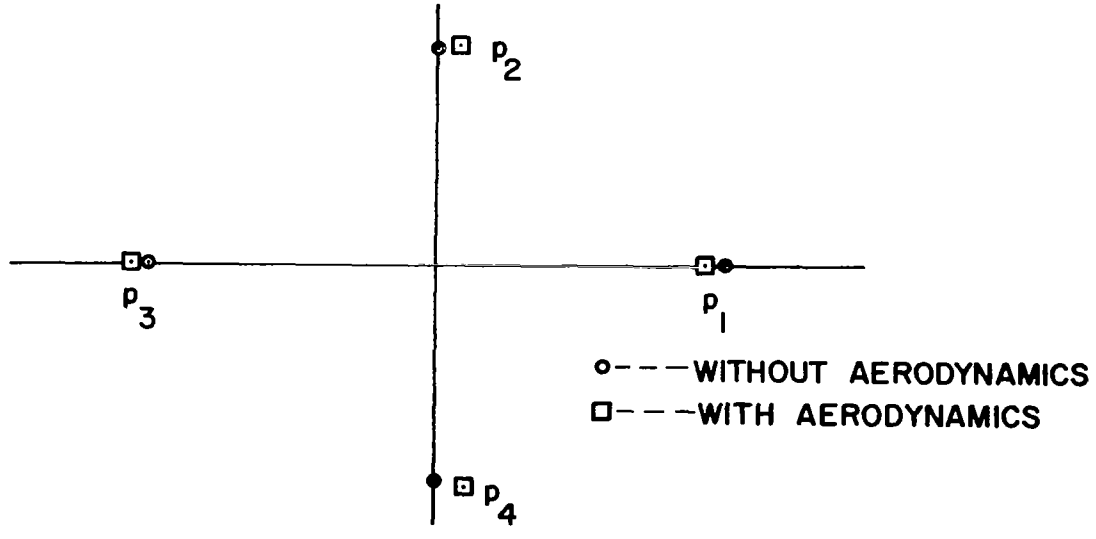

FIGURE 2c. ROOT SHIFT DUE TO AERODYNAMIC FORCES; μ = 58.0, η = 810, M = 1.35, g = 0.01, k = 0.65.

that there are four such pairs with two additional roots (numbered 5 and 10) that are nearly pure imaginary except for small real shifts due to damping. The two imaginary roots always lie close to the branch cut between the two branch points A and B.

From the form of (2.16), we conclude that each of the ten roots is either a root of $\bar{D}^+$ or $\bar{D}^-$. The number of roots of each factor depends upon the choice of branch cut used to make the factor $h^{\frac{1}{2}}(p)$ single valued. In the following discussion, we choose the branch cut to be the straight line between the branch points p_A and p_B. This choice assigns five roots to each factor. In Fig. 2a the + or - sign near each root indicates which one is a zero of $\bar{D}^+$ or $\bar{D}^-$. In our subsequent discussion, we concentrate on the interpretation of the roots of $\bar{D}^+$.

The structural roots of $\bar{D}^+$

When the aerodynamic term is dropped in (2.6), then $\bar{D}^+$ has four roots (zeroes of the polynomial $g(p)$) that lie on the real and imaginary axes (for $g = 0$), as shown in Fig. 2b. This is the limiting configuration of the first four roots of $\bar{D}^+$ as the dynamic pressure tends to zero. We shall refer to roots 1,2,3,4 as the structural roots of $\bar{D}^+$.

Initial membrane stresses have a significant effect on the structural roots. In particular, a chordwise membrane tensile stress, r_{x_o}, shifts the roots 1 and 3 out on the real axis whereas a compressive stress shifts them toward the origin (Fig. 2b). In the limit of very large tensile membrane stress, these two roots tend to plus and minus infinity, respectively. The roots 2 and 4 are shifted in exactly the opposite sense of roots 1 and 3.

Aerodynamic forces cause the structural roots to shift as shown in Fig. 2c. The roots 1 and 3 shift to the left and acquire small imaginary parts, whereas the roots 2 and 4 shift to the right. The principal contribution to this root shift is the aerodynamic stiffness. Damping (aerodynamic, structural or viscous) has a very small effect on root location. However, we

shall see that the small damping shifts have a profound effect on the traveling-wave type of flutter.

It is important to understand the structural root shifts as a function of reduced frequency k and mass ratio parameter $\mu = \rho_s \tau / \rho_\infty$. For fixed μ sufficiently small, the roots shift with k as follows (see Fig. 3a). For small k (of the order of a few tenths), the roots p_2 , p_4 are to the right of p_1 . For increasing k , p_2 and p_4 shift to the left of p_1 and their imaginary parts increase, as shown in Fig. 3a. For some larger critical value of μ , the roots p_2 and p_4 can never get to the right of p_1 for any value of k . This critical value of μ we shall call $\mu_{s.w.}$. We shall see that $\mu_{s.w.}$ is the largest value of μ for which standing-wave type of flutter can occur in a very long panel. Furthermore, standing-wave flutter only occurs when k is such that the real parts of the roots p_1 , p_2 and p_4 are close together. The degree of proximity depends upon the length-to-width ratio. The foregoing phenomena is not affected appreciably by small amounts of damping (aerodynamic, structural or viscous).

Applied membrane stresses have a significant effect on the root shifts due to aerodynamic stiffness. A tensile stress shifts the root p_1 to the right on the real axis so that more aerodynamic stiffness (higher dynamic pressure) is needed to cause standing-wave flutter. In the limit of a very large tensile stress (pure membrane panel), p_1 is shifted to infinity so that standing-wave flutter cannot occur at all. Only flutter of the traveling-wave type can occur in the membrane. On the other hand, a compressive stress shifts p_1 toward the origin so that less aerodynamic stiffness is needed for flutter.

For larger values of k (order unity or greater) and fixed $\mu > \mu_{s.w.}$, we have the following situation. With increasing k, the roots p_2 and p_4 tend to the imaginary axis. The imaginary parts of p_2 and p_4 get larger as do the branch points p_A and p_B . For each μ there is, in general, a finite k-band where

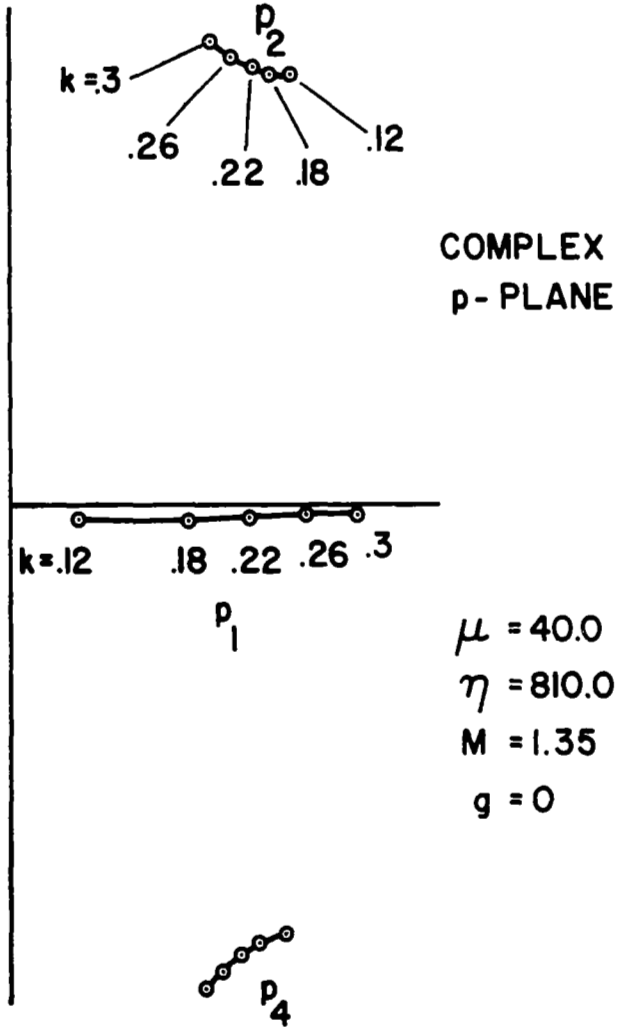

FIGURE 3a. ROOT SHIFT WITH REDUCED FREQUENCY FOR $\mu < \mu_{s.w.}$

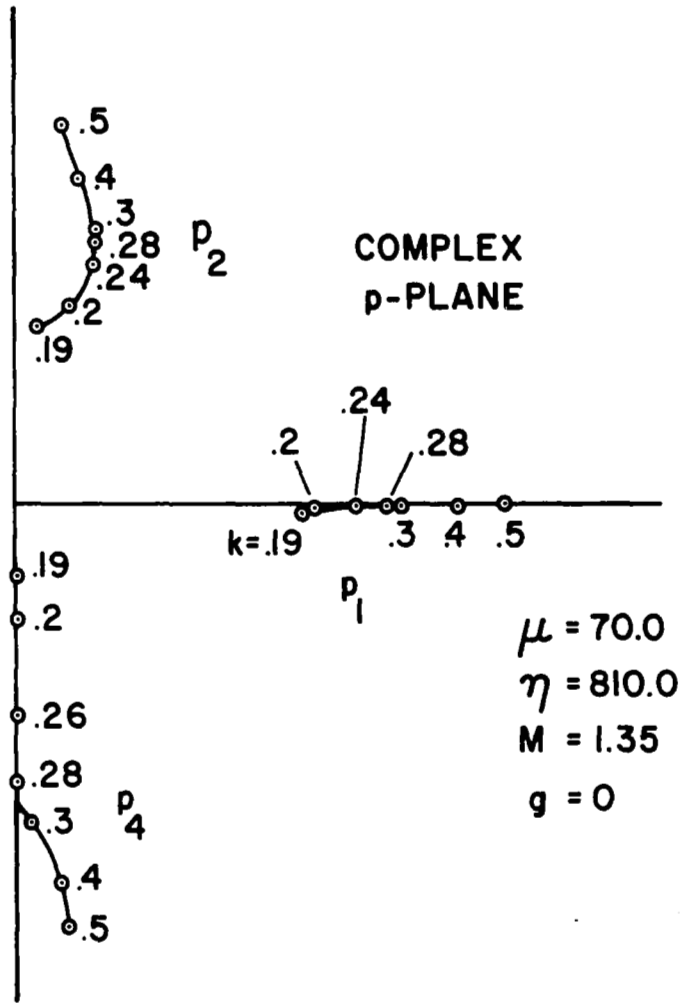

FIGURE 3b. ROOT SHIFT WITH REDUCED FREQUENCY FOR $\mu > \mu_{s.w.}$

the Re $p_4 >$ Re p_2 . Near each end of the k-band, this inequality reverses and, in fact, Re p_4 becomes nearly zero (see Fig. 3b). The size of the k-band diminishes with increasing μ until a value $\mu_{t.w.}$ is reached for which a finite band does not exist. Flutter of the traveling-wave type occurs in each k-band and, in fact, the limiting value $\mu_{t.w.}$ coincides precisely with the so-called "traveling-wave theory" for an infinite length panel. This type of flutter depends upon the existence of a k-band for which Re $p_4 >$ Re p_2 . In general, very small amounts of structural damping eliminate the possibility of this type of flutter except in the low Mach number range or for very long panels. The reason is that a positive amount of g increases Re p_2 and decreases Re p_4 slightly so that the relevant inequality (Re $p_4 >$ Re p_2) can never be satisfied. This is in sharp contrast to the standing-wave type which is relatively insensitive to small damping values.

Interpretation of the roots

Each of the roots of $\bar{D}^+$ has a simple physical interpretation that helps to understand the flutter solution. Consider once again the simple example when the aerodynamic forces are dropped. Then each of the four roots p_1, p_2, p_3, p_4 yields a simple exponential solution, $e^{p_n x}$, of the beam equation. If we combine the exponential with the time dependence, each solution is of the form

$$e^{p_n x + ikt}$$

The roots p_2 and p_4 can be interpreted as pure traveling waves. Here p_2 travels in the negative x direction (toward the leading edge) and p_4 travels in the positive x direction (toward the trailing edge). The root p_1 decays exponentially in the negative x direction and so is important only at the trailing edge when the panel is long. Conversely, p_3 decays exponentially in the positive x direction and so is important at the leading edge. The roots p_1 and p_3 are important for the reflection of traveling waves at the trailing and leading edges, respectively.

Exactly the same interpretation can be assigned to the structural roots of $\bar{D}^+$. Now, however, the roots p_2 and p_4 have positive real parts so that they both decay exponentially in the negative x direction. This decay leads to the concentration of the flutter mode toward the trailing edge.

The fifth root of $\bar{D}^+$ is wholly aerodynamic in origin. It lies near the branch cut and is nearly pure negative imaginary. Thus, it can be interpreted as a wave traveling toward the trailing edge.

Interpretation of the branch points

The branch points p_A and p_B also have a physical interpretation. (Recall they are singularities in the transformed pressure (2.4).) For an infinite length panel, the basic panel flutter equation (1.16) has pure exponential solutions of the form e^{px}. Thus $\bar{P}(p)$ in (2.4) is the actual pressure amplitude for an exponential type solution. Further, if we set $p = -2\pi i/\lambda$, then $\bar{P}$ is the pressure amplitude for a pure traveling-wave mode shape of wave length λ. The branch points are combinations of λ, k and M where the pressure amplitude becomes infinite. We have

$$\frac{2\pi}{\lambda} = -KM \pm \Gamma$$

$$= \pm \frac{\sqrt{c_2}}{\beta} \qquad \text{steady flow}$$

When the flow is steady and the surface wave pattern is stationary ($k = 0$), we obtain the critical surface pattern wave length for which the pressure becomes infinite. This "pattern singularity" is the aerodynamic mechanism to which the phenomenon of pattern ablation is attributed (see Ref. 19).

For traveling-wave type flutter, the structural root p_4 is often very close to the branch point p_B. Although the phenomenon is not fully understood, the necessary root shift to obtain traveling-wave flutter appears to be augmented by the proximity of p_4 to this pattern singularity.

III. ASYMPTOTIC RESULTS

A. General Theory for $s \to \infty$

Even though we have an exact analytic solution of the flutter problem in hand, it is very useful and informative to consider the asymptotic approximation for long panels. The approximation is exact in the limit ($s \to \infty$) and is useful for numerical evaluation of flutter boundaries and mode shapes. Also, new insights into the mechanisms of "standing-wave" and "traveling-wave" type flutter are obtained.

The point of departure for the general theory as $s \to \infty$ is the characteristic function $F(x)$ or rather the ten individual functions $F_n(x)$ of which it is composed (see (2.19) and (2.20)). To develop an asymptotic flutter condition (see (2.25) and (2.26)), we must first expand each $F_n(s)$ for $s \to \infty$. This is a straightforward operation since we have an explicit definition of each function in (2.20). The results are summarized below:

$$\begin{aligned} F_n(s) &= 2A_n e^{p_n s} + \bar{F}_n(s) \qquad n = 1,2,3,4,5 \\ &= \bar{F}_n(s) \qquad n = 6,7,8,9,10 \end{aligned} \tag{3.1}$$

where

$$\frac{1}{2A_n} = g'(p_n) + \left\{\frac{\ell'(p_n)}{\ell(p_n)} - \frac{h'(p_n)}{2h(p_n)}\right\} g(p_n) \tag{3.2}$$

$$\bar{F}_n(s) = \frac{\ell(p_n)A_n}{g(p_n)}\, e^{p_n s}\, \bar{G}_n(s) \tag{3.3}$$

and $\bar{G}_n(s)$ is given in Appendix B where the functions $F_n(s)$ are evaluated in general. For $s \to \infty$, there are two distinct cases to consider that we call the standing-wave limit and traveling-wave limit.

B. Standing-Wave Limit

When the real parts of the structural roots p_1, p_2, p_4 are of the same order of magnitude, then the only three characteristic functions of importance are F_1, F_2, F_4. Their asymptotic forms are

$$F_n(s) = 2A_n e^{p_n s} + O(1) \qquad n = 1,2,4 \tag{3.4}$$

and

$$F(s) = \sum_{n=1,2,4} C_n e^{p_n s} + O(1) \tag{3.5}$$

This is the form of the characteristic function for the standing-wave branch of the flutter boundary where, in fact,

$$\text{Re } p_1 \cong \text{Re } p_2 \cong \text{Re } p_4 \quad \text{for} \quad s \to \infty \tag{3.6}$$

The formulae obtained in the standing-wave limit are strong asymptotic results in that corrections are $O\{\exp(-\text{Re } p_n s)\}$ compared to unity.

The flutter determinant and mode shapes for pinned and clamped edges have the following asymptotic forms:

Pinned Edges

$$D(k,s) \sim 1 + \frac{A_4}{A_2} e^{(p_4-p_2)s} \cdot \left(\frac{p_1^2 - p_4^2}{p_1^2 - p_2^2}\right)^2 + \frac{A_4}{A_1} e^{(p_4-p_1)s} \cdot \left(\frac{p_2^2 - p_4^2}{p_1^2 - p_2^2}\right)^2 = 0$$

$$f^{(m)}(s - X) \sim \left(p_1^m e^{-p_1 X} + p_2^m e^{-p_2 X}\right) +$$

$$+ \frac{A_4}{A_2} e^{(p_4-p_2)s} \left(\frac{p_1^2 - p_4^2}{p_1^2 - p_2^2}\right)\left(p_1^m e^{-p_1 X} + p_4^m e^{-p_4 X}\right) +$$

$$+ \frac{A_4}{A_1} e^{(p_4-p_1)s} \left(\frac{p_2^2 - p_4^2}{p_1^2 - p_2^2}\right)\left(p_2^m e^{-p_2 X} + p_4^m e^{-p_4 X}\right) \tag{3.7}$$

Clamped Edges

$$D(k,s) \sim 1 + \frac{A_4}{A_2} e^{(p_4-p_2)s} \left(\frac{p_1 - p_4}{p_1 - p_2}\right)^2 +$$

$$+ \frac{A_4}{A_1} e^{(p_4-p_1)s} \left(\frac{p_2 - p_4}{p_1 - p_2}\right)^2 = 0$$

$$f^{(m)}(s - X) \sim p_1^m e^{-p_1 X} + p_2^m e^{-p_2 X} +$$

$$+ \frac{A_4}{A_2} e^{(p_4-p_2)s} \left(\frac{p_1 - p_4}{p_1 - p_2}\right)\left(p_1^m e^{-p_1 X} + p_4^m e^{-p_4 X}\right) +$$

$$+ \frac{A_4}{A_1} e^{(p_4-p_1)s} \left(\frac{p_2 - p_4}{p_1 - p_2}\right)\left(p_2^m e^{-p_2 X} + p_4^m e^{-p_4 X}\right) \tag{3.8}$$

where X is the distance from the trailing edge. Note that the mode shape is exponentially small near the leading edge.

If we examine the further limit of (3.7) and (3.8) as $M \to \infty$ and $k \to 0$ we obtain the well-known approximations for quasi-steady and static aerodynamic theory for large s. We have

Quasi-Steady Theory

$$\bar{D}^{+}(p) = g(p) + \frac{S}{\beta}\left(p + ik\,\frac{M^2 - 2}{M^2 - 1}\right) \tag{3.9}$$

Static Theory

$$\bar{D}^{+}(p) = g(p) + \frac{S}{\beta}\,p \tag{3.10}$$

For either case

$$\frac{1}{2A_n} = g'(p_n) + \frac{S}{\beta}$$

$$= 4p_n^3 - 2Ap_n + \frac{S}{\beta} \tag{3.11}$$

The results (3.7) and (3.8) are much stronger than the quasi-steady and static theory approximations. They are valid for arbitrary Mach number so long as s is large. There is only a minor difference in computational labor from the simpler theories; i.e., we must calculate the three roots p_1, p_2, p_4 from the zeroes of $\bar{D}^{+}$ rather than the simple fourth order polynomial (3.9) or (3.10). Finally we remark that the reason for naming (3.7) and (3.8) "standing-wave" results is that we recover the simple static theory in the limit. The actual mode shape will, in general, have a traveling-wave component when damping is present.

C. Traveling-Wave Limit

Another important limiting case is obtained when the structural roots p_2 and p_4 lie close to the imaginary axis and p_1 is well out on the real axis. In this case, the large exponential part of the characteristic function F_1 must be removed, essentially since it is the difference between lower order terms that leads to flutter. For the flutter determinants (2.25) and (2.26) to vanish, the coefficient of the function $F_1 \sim 2A_1 e^{p_1 x}$ must be set to zero. This leads to a single

summation over the remaining functions; namely,

$$D(k,s) \sim \sum_{n=2}^{10} F_n(s) \left(p_1^2 - p_n^2\right)^2 = 0 \quad \text{pinned edges}$$

$$\sim \sum_{n=2}^{10} F_n(s) \left(p_1 - p_n\right)^2 = 0 \quad \text{clamped edges} \qquad (3.12)$$

In general, all of the remaining functions F_2 through F_{10} contribute to $D(k,s)$. An important special case where only two terms contribute is considered in the next section.

To derive asymptotic formulae for the mode shapes, we write the characteristic function in the form

$$F(x) = 2A_1 e^{p_1 x} + \bar{F}(x) \qquad (3.13)$$

and substitute into the formulae (2.8). We get

$$f(x) = 2A_1 \left[\left(p_1^2 - A\right) f_o' + f_o'''\right] e^{p_1 x}$$

$$+ \left(\bar{F}'' - A\bar{F}\right) f_o' + \bar{F} f_o''' \qquad \text{pinned}$$

$$f(x) = 2A_1 \left[p_1 f_o'' + f_o'''\right] e^{p_1 x} + \left(\bar{F}' f_o'' + \bar{F} f_o'''\right) \text{ clamped} \qquad (3.14)$$

Now apply the boundary condition at the trailing edge for large s . We obtain

$$\frac{f_o'}{f_o'''} = - \frac{2A_1 + \bar{F}(s) e^{-p_1 s}}{2A_1\left(p_1^2 - A\right) + \left(\bar{F}''(s) - A\bar{F}(s)\right) e^{-p_1 s}} \qquad \text{pinned}$$

$$\frac{f_o''}{f_o'''} = - \frac{2A_1 + \bar{F}(s) e^{-p_1 s}}{2A_1 p_1 + \bar{F}'(s) e^{-p_1 s}} \qquad \text{clamped} \qquad (3.15)$$

Substitute (3.15) into (3.14) and expand for large s to obtain

$$f(x) = \left[\bar{F}''(s) - p_1^2\bar{F}(s)\right] e^{-p_1(s-x)} - \bar{F}''(x) + p_1^2\bar{F}(x) \quad \text{pinned}$$

$$f(x) = \left[\bar{F}'(s) - p_1\bar{F}(s)\right] e^{-p_1(s-x)} - \bar{F}'(x) + p_1\bar{F}(x) \quad \text{clamped} \tag{3.16}$$

The effect of the exponential part of F_1 is only important near the trailing edge where it is needed for reflection of the incident traveling wave.

The foregoing approximation is again a strong asymptotic result in that corrections are of $O\left(e^{-p_1 s}\right)$ compared to unity. Where flutter is obtained within this approximation it is of the traveling-wave type.

D. A Weak Traveling-Wave Limit

A special case of the traveling-wave result is obtained when $\text{Re } p_2 \cong \text{Re } p_4$ and both roots are close to, but not on, the imaginary axis. Also, we must have s sufficiently large that we can neglect terms of $O\left(e^{-p_2 s}\right)$ compared to unity. In this sense, the following results are weakly asymptotic. However, they serve to illustrate some of the basic properties of traveling-wave type of flutter.

For the case at hand, we can neglect all but the exponential part of the terms F_2 and F_4 in (3.12). Alternatively, we obtain the same result for $D(k,s)$ if we neglect the last term in (3.7) and (3.8). Thus we have for the flutter condition

$$-\frac{A_4}{A_2}\left(\frac{p_1^2 - p_4^2}{p_1^2 - p_2^2}\right)^2 e^{(p_4-p_2)s} = 1 \quad \text{pinned}$$

$$-\frac{A_4}{A_2}\left(\frac{p_1 - p_4}{p_1 - p_2}\right)^2 e^{(p_4-p_2)s} = 1 \quad \text{clamped} \tag{3.17}$$

Each of these can be solved completely. Let

$$p_n = a_n + i\, b_n$$

and

$$Re^{i\phi} = -\frac{A_4}{A_2}\left(\frac{p_1^2 - p_4^2}{p_1^2 - p_2^2}\right)^2 \qquad \text{pinned}$$

$$= -\frac{A_4}{A_2}\left(\frac{p_1 - p_4}{p_1 - p_2}\right)^2 \qquad \text{clamped} \tag{3.18}$$

Then for either of (3.17) we have

$$Re^{(a_4-a_2)s} \cdot e^{i[(b_4-b_2)s+\phi]} = 1$$

or separating real and imaginary parts

$$Re^{(a_4-a_2)s} \cos\left[(b_4 - b_2)s + \phi\right] = 1$$

$$\sin\left[(b_4 - b_2)s + \phi\right] = 0 \tag{3.19}$$

From the second equation we have

$$(b_2 - b_4)s - \phi = 2m\pi \qquad m = 1,2,\ldots$$

and upon substitution in the first of (3.19), we get

$$s = \frac{1}{a_4 - a_2} \log R$$

In summary, we have the following equations for s :

$$s = \frac{2m\pi + \phi}{b_2 - b_4} \qquad m = 1,2,\ldots \qquad \text{(a)}$$

$$s = \frac{\log R}{a_4 - a_2} \qquad \text{(b)} \qquad (3.20)$$

where R and ϕ are defined by (3.18). The intersection of (3.20b) with the branches of (3.20a) yields an infinite set of flutter points. Whether or not flutter of this type is possible at all depends upon the algebraic sign of $a_4 - a_2$. We shall see by numerical example in Section IV that such flutter is possible, but that it is very sensitive to damping. Mach number and other small changes that can switch the sign of $a_4 - a_2$.

E. Infinite Length Static Theory

Here we give a limit result that is based on the simple static aerodynamic theory (see (3.10). When there is no damping of any kind it is found by numerical calculation that flutter based on static aerodynamic theory with $s \to \infty$ occurs when the roots p_2 and p_4 coalesce with p_1 on the real axis. In such case, the characteristic polynomial and its first two derivatives must vanish simultaneously to yield a triple root. Thus

$$\begin{aligned} p^4 - Ap^2 + \frac{S}{\beta} p + B &= 0 \\ 4p^3 - 2Ap + \frac{S}{\beta} &= 0 \\ 6p^2 - A &= 0 \end{aligned} \qquad (3.21)$$

These equations are easily solved for the root p_1 and other physical parameters at flutter. The result is:

$$p_1 = \left(\frac{C_2\Omega_{xy}}{3} + \frac{r_x}{6}\right)^{1/2}$$

$$\mu_{s.w.} = \frac{1}{p_1}\left(\frac{3M^2\eta^2}{2\beta}\right)^{1/3}$$

$$k_{s.w.} = \frac{p_1}{2}\left(\frac{3}{2M\beta\eta}\right)^{1/3}\left\{1 + \frac{C_2\Omega_{xy} + r_y}{C_2\Omega_{xy}\left(1 + \frac{r_x}{2C_2\Omega_{xy}}\right)^2}\right\}^{1/2}$$

$$r_x = r_{x_o} + r_{x_1}\ ,\ r_y = r_{y_o} + r_{y_1} \qquad (3.22)$$

where

$$\mu = \frac{\tau\rho_s}{\rho_\infty} = \frac{R}{S_o} \qquad \text{mass ratio parameter}$$

$$\eta = \frac{\rho_s a_\infty}{\rho_\infty a_s} = \frac{1}{M}\left(\frac{S_o\mu^3}{12}\right)^{1/2} \qquad \text{material altitude parameter}$$

$$a_s = \left[\frac{E}{\rho_s(1 - \nu^2)}\right]^{1/2} \qquad \text{speed of sound in the panel material}$$

(3.23)

The results (3.22) are useful for numerical calculations with the exact formulae since they yield an approximate upper bound on μ for which standing-wave type of flutter can occur.

Also, one can see immediately the effect of edge restraint, membrane stress, Mach number, material and altitude on flutter thickness or μ value. When $r_x = 0$, we have

$$p_1 = \frac{\pi}{\sqrt{3}} = 1.81 \qquad \text{pinned edges}$$

$$= \frac{3.49}{\sqrt{3}} = 2.02 \qquad \text{clamped edges}$$

Clamping the stringers causes about a 10% reduction in the pinned edge flutter μ. Membrane tension causes an increase in p_1 and a reduction in $\mu_{s.w.}$, while compression has the opposite effect. Also, we see that $\mu_{s.w.}$ increases as $M^{1/3}$ for large M and increases as $\eta^{2/3}$. Dense materials with low sound speeds at high altitude require greater μ for stability. Both cases, however, require smaller panel thickness.

F. Semi-Infinite Traveling-Wave Theory

In Ref. 20 Dowell treated the infinite length discrete panel, and in Ref. 21 some results for the panel array are given. A comparison of the traveling-wave results with exact calculations for very long panels (see Section IV) suggests that "traveling-wave theory" is a valid limit of the exact theory (at least when structural damping is absent). Assuming that the traveling-wave theory is a valid limit (a theoretical proof is lacking) we can construct the solution of a semi-infinite panel array that has its leading edge upstream at infinity and a trailing edge at the origin.

The flutter boundary for the semi-infinite panel array is the same as that for an infinite length array. The detailed method of calculation is discussed by Dowell (Ref. 20). Here we summarize a convenient parametric method. If t is a parameter ranging from 1 to infinity, the formulae are:

$$a = \frac{2\pi\mu}{t^{\frac{1}{2}}(1+t)} \qquad b = \left(1 - \frac{1}{t}\right)^{\frac{1}{2}} \qquad d = \frac{2a}{1+t}$$

$$x = b\left(\frac{M/a + \sqrt{M^2 - b^2 + b^2/a^2}}{M^2 - b^2}\right) \qquad y = \left(\bar{n}^2 + x^2\right)^{\frac{1}{2}}$$

$$c^* = \frac{\left[y^4 + r_x(y^2 - \bar{n}^2)/\pi^2 + \bar{n}^2 r_y/\pi^2\right]^{\frac{1}{2}}}{2x(1 \pm dy)^{\frac{1}{2}}} \qquad \text{wave speed}$$

$$U^* = (1 + ay)c^* \qquad \text{flutter speed}$$

$$\lambda = \frac{2}{x} \qquad \text{wave length} \tag{3.24}$$

where

$$c^* = \frac{c}{c_o} \qquad U^* = \frac{U}{c_o}$$

$$c_o = 2\pi \left(\frac{D}{\rho_s \tau}\right)^{\frac{1}{2}} \qquad \text{reference wave speed} \tag{3.25}$$

For fixed values of M, μ, $\bar{n}$, r_x, r_y, we calculate the minimum of U^* as a function of the parameter t. The resultant value is the flutter speed.

The main point of interest here is the calculation of the mode shape. Recall that the infinite length mode shape is simply a sine wave traveling in the stream direction with velocity c^*. We ask what happens when the wave approaches the trailing edge.

Referring once again to the root plane, Fig. 2a, we note first that the traveling-wave root is the root p_4; i.e., the wave length, $\lambda = 2\pi/|p_4|$. When $\mu = \mu_{t.w.}$, as computed from (3.24), p_4 is pure negative imaginary. For an infinite panel p_4 is the only admissable root in that the corresponding eigenfunction $e^{p_4 X}$ does not grow or decay in the upstream or downstream direction. For the semi-infinite panel, the roots p_1 and p_2 are also admissable solutions; i.e., we can write the mode shape of the semi-infinite panel in the form

$$f(x) = e^{-p_4 X} + A_1 e^{-p_1 X} + A_2 e^{-p_2 X} \tag{3.26}$$

where X is the distance measured upstream from the trailing edge. We have normalized f such that it tends asymptotically to a unit amplitude sine wave at upstream infinity. Now apply the boundary condition at the trailing edge

$$-\epsilon_c f'(0) + \epsilon_p f''(0) = 0 \tag{3.27}$$

The final result for A_1 and A_2 is

$$A_1 = \frac{u_4 - u_2}{u_2 - u_1} \qquad A_2 = \frac{u_1 - u_4}{u_2 - u_1}$$

$$u_n = \epsilon_c p_n + \epsilon_p p_n^2 \qquad n = 1,2,4 \tag{3.28}$$

To calculate the mode shape for a semi-infinite panel the procedure is the following:

1. Calculate a traveling-wave flutter point using (3.24).
2. For the flutter point obtained in step 1, calculate all roots of the characteristic function $\bar{D}^+$ (see Eq. (2.6) and isolate p_1 and p_2. Recall p_4 is obtained in step 1.
3. Use the roots to calculate the mode shape with (3.26).

Numerical calculations are given in Section IV.

IV. NUMERICAL RESULTS

A. Description and Verification of the Computational Scheme

In the present section, we show how flutter calculations are made with the Zeydel method and give some comparisons with previous results that verify the computational scheme. In all calculations presented, the following conditions hold:

1. Pinned leading and trailing edges;
2. Stringers without torsional restraint (pinned);
3. Isotropic panel material ($\Omega_{xy} = \Omega_{yy} = 1$);
4. Zero viscous damping ($\gamma = 0$);
5. No elastic foundation ($K_e = 0$).

A complete discussion of the dimensionless parameters used to display numerical results is given in Appendix C, together with some useful formulae for conversion to dimensional quantities.

The k versus s parameter plane is used to search for flutter points on the computer. Typical results are given in Fig. 4 and are calculated as follows. The parameters M, μ, η, g, r_x, and r_y are fixed. Then, the flutter condition (see (2.25) and (2.26)) is expressed in the form

$$D(k,s) = D_R(k,s) + i\, D_I(k,s) = 0 \qquad (4.1)$$

where D_R and D_I are the real and imaginary parts of D. The solid curves in Fig. 4 are the locus of points where $D_R = 0$. There are an infinite number of branches of D_R of which the first ten are shown (labelled $m = 1,2,\ldots$). The branch index m is the number of half waves in the deflection mode and may be put into one-to-one correspondence with the natural vibration modes. In fact, the branches tend asymptotically to the locus of natural frequencies of the panel for large k or for vanishing aerodynamic forces.

The actual flutter points in Fig. 4 are obtained as follows.

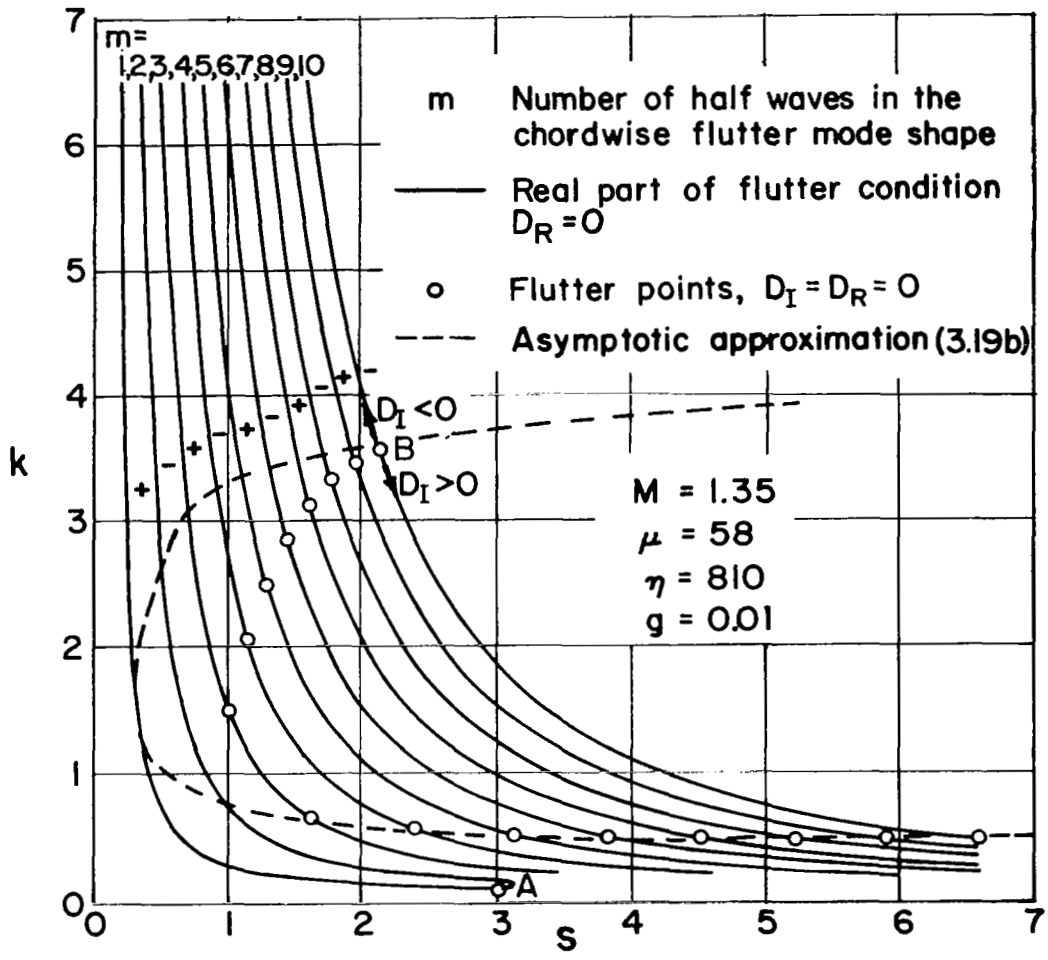

FIGURE 4. COMPUTER PARAMETER PLANE (k versus s) AND TYPICAL CALCULATION OF FLUTTER POINTS

The value of $D_I(k,s)$ is computed along each branch for different k values. When D_I changes sign at two consecutive points on any branch, we iterate for the flutter point that lies in between. There are two distinct types of flutter points that are obtained in this way (see points A and B in Fig. 4):

Standing-wave flutter (Point A, Figure 4)

The sign of $D_I(k,s)$ alternates as we traverse successive branches. Furthermore, if μ is sufficiently small, as it is in Fig. 4, then the branches coalesce in pairs (1 and 2), (3 and 4), etc., for small k (of the order of a few tenths). At each point of coalescence, D_I is zero and we obtain a flutter point.

The coalescence at point A , for example, in Fig. 4 is the coalescence of frequencies of branches (or modes) 1 and 2 as the length-to-width ratio is varied. The boot of the k-s plane is, in fact, just a new way of displaying the well known frequency coalescence type of flutter that is characterized by strongly coupled modes and a nearly standing wave type of mode shape. We refer to this type of flutter as standing-wave flutter in the present study, even though it is only in the absence of all damping that the mode shape is a pure standing wave.

The standing-wave flutter points are approximated closely by the simple static aerodynamic theory with zero structural damping even at fairly low values of the Mach number. Subsequent results will substantiate this claim. The largest value of μ for which standing-wave flutter can occur is therefore given approximately by $\mu_{s.w.}$ in (3.21). For example, for the values of M and η in Fig. 4, the largest value of μ is approximately 69.3 . Beyond this value of μ , the branches do not coalesce in the k versus s plane.

Traveling-wave flutter (Point B, Figure 4)

The second type of flutter is obtained for larger values of k and occurs in pairs on successive branches. There is always a lowest branch for which it can occur at all;e.g., it is branch 3 in Fig. 4. All of the flutter points occur in a finite k-band.

In Fig. 4, k lies between .5 and 3.7 . As μ is increased, the k-band decreases to zero at some limiting value $\mu = \mu_{t.w.}$, and the lowest branch number for flutter tends to infinity. We shall see, by numerical example, that the limiting value is predicted by the simple traveling-wave theory" (Refs. 20, 21) for an infinite length panel when $g = 0$. It is for this reason that we have chosen to identify the second type of flutter as traveling-wave flutter.

In Table 1, a comparison is made of flutter points calculated by the Galerkin method (Ref. 22) and the present exact method for a square panel at $M = 1.35$.

TABLE 1. COMPARISON OF GALERKIN AND EXACT RESULTS
($g = .01$, $r_x = r_y = 0$)

μ	δ	k		s	
		Galerkin	Exact	Galerkin	Exact
58.02	84.227	1.50	1.49997	1.0	.99998
38.86	59.147	1.70	1.69942	1.0	1.00017
28.70	46.386	1.80	1.79843	1.0	1.00049
17.63	32.127	1.90	1.89412	1.0	1.00181

We conclude from Table 1 that: (1) the Galerkin procedure gave converged results for the case considered in Ref. 22, and (2) the present exact scheme is calculating correctly. Further verification is to be found in the nature of the mode shape. In Ref. 22, it is pointed out that the third mode is dominant in the Galerkin calculations. With the exact procedure, flutter occurs in every case on branch 3. The actual mode shape for the first point in Table 1 is given in Fig. 5. It is clearly dominated by the third "assumed mode." Finally, we remark that all flutter points in Table 1 are of the traveling-wave type and form part of the critical flutter branch.

B. Effect of Altitude and Panel Material on Flutter Boundaries

For a given set of μ values, the k-s plane calculations

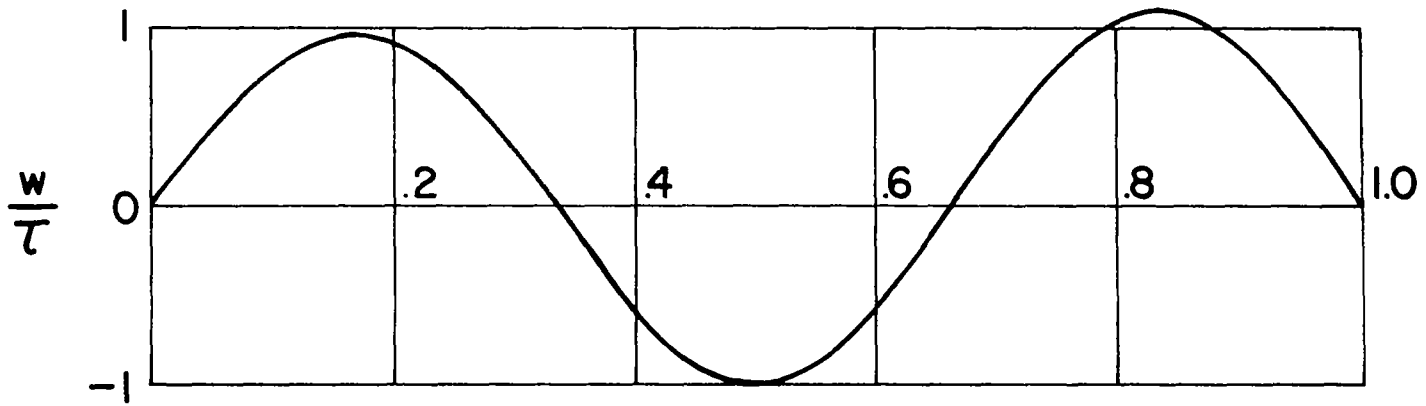

FIGURE 5. TYPICAL TRAVELING-WAVE FLUTTER MODE SHAPE FOR A SQUARE PANEL; $M = 1.35$, $\mu = 58.02$, $\delta = 84.227$, $g = 0.01$, $k = 1.5$

are repeated to obtain design curves of μ versus s . Results are given in Figs. 6a, b, c, and d for four values of the material altitude parameter η at $M = 1.35$. For any panel material, the conversion of these data to thickness versus panel length is straightforward. The detailed procedure is given in Appendix C.

The present computational scheme has the advantage of giving a complete curve for all length-to-width ratios. We note that for all of the results in Fig. 6 the maximum thickness required to prevent flutter is required by the very long panels. Both the standing- and traveling-wave branches of the flutter boundary have this property. We conclude that a very conservative estimate of the design thickness of a panel can be calculated from results for $s = \infty$.

The traveling - wave branch of the flutter boundary consists of a series of loops in the μ vs. s plane. The practical stability boundary is the envelope of these loops. Each loop corresponds to one of the branch numbers on a k vs. s graph like Fig. 4. Thus, for any value of s , we can simply read off the number of half waves in the mode shape, as well as the μ value at flutter.

The envelope of the traveling wave loops tends to a limiting value in each of the curves of Fig. 6. This limit is in all cases very close to the flutter $\mu_{t.w.}$ predicted by the "traveling - wave" theory of an infinite length array of panels (Ref. 21). Also, the wave length is calculated to be about one panel width in each case. The result based on "traveling-wave" theory with $g = 0$ is included on each curve of Fig. 6. In all cases, the present results tend to asymptote slightly below the $g = 0$ limit value. These results indicate that true structural damping has a stabilizing effect on the traveling wave flutter branch. Recall the result of Dowell (Ref. 20) that any small amount of viscous-type damping always leads to instability when $M > 1$.

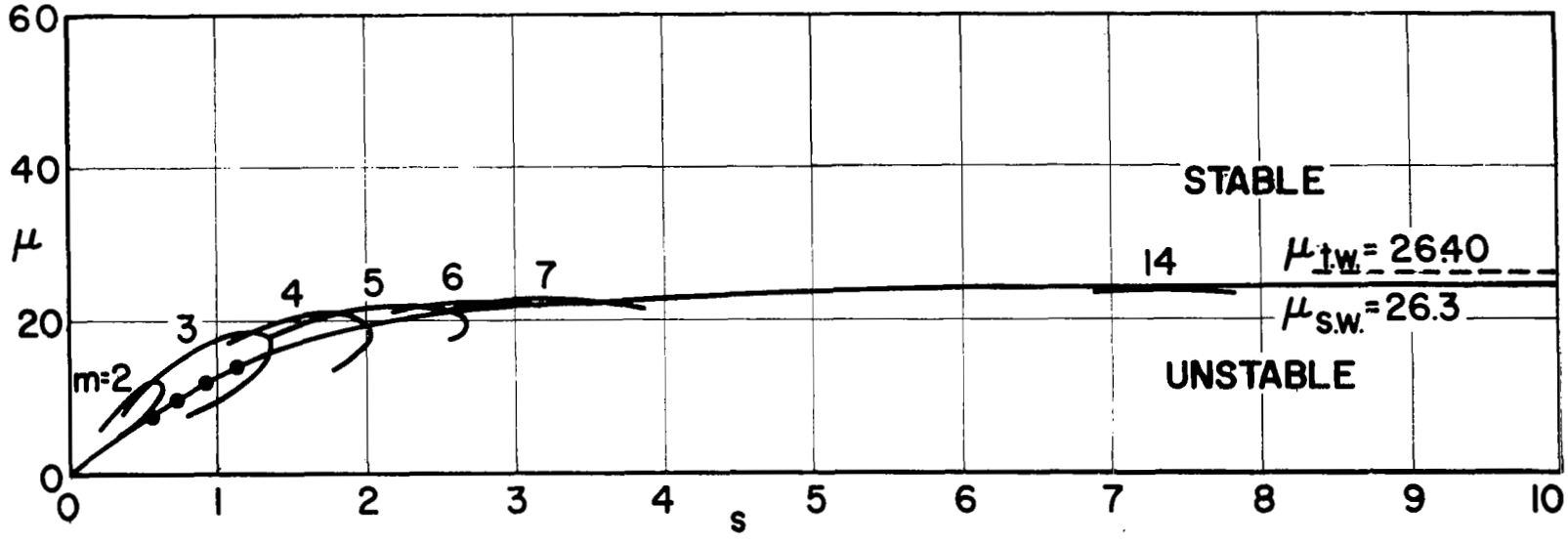

FIGURE 6a. DESIGN FLUTTER BOUNDARY (μ versus s); M = 1.35 , η = 190.76 , g = 0.01

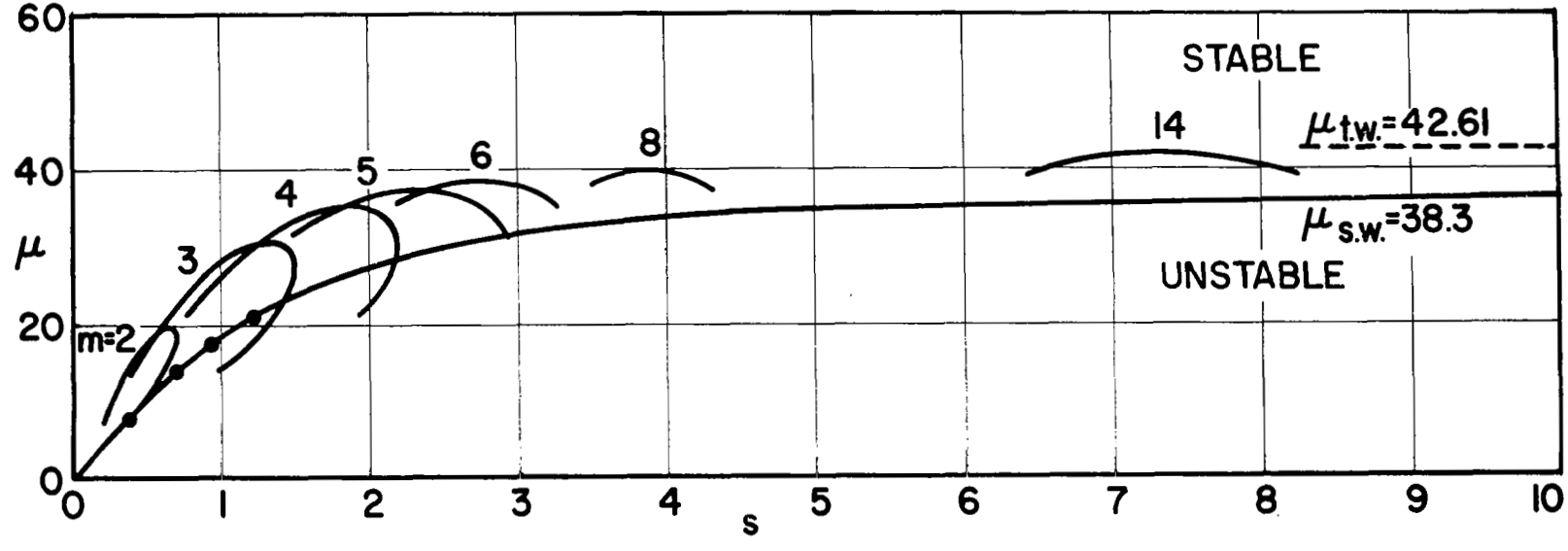

FIGURE 6b. DESIGN FLUTTER BOUNDARY (μ versus s); M = 1.35 , η = 330.95 , g = 0.01

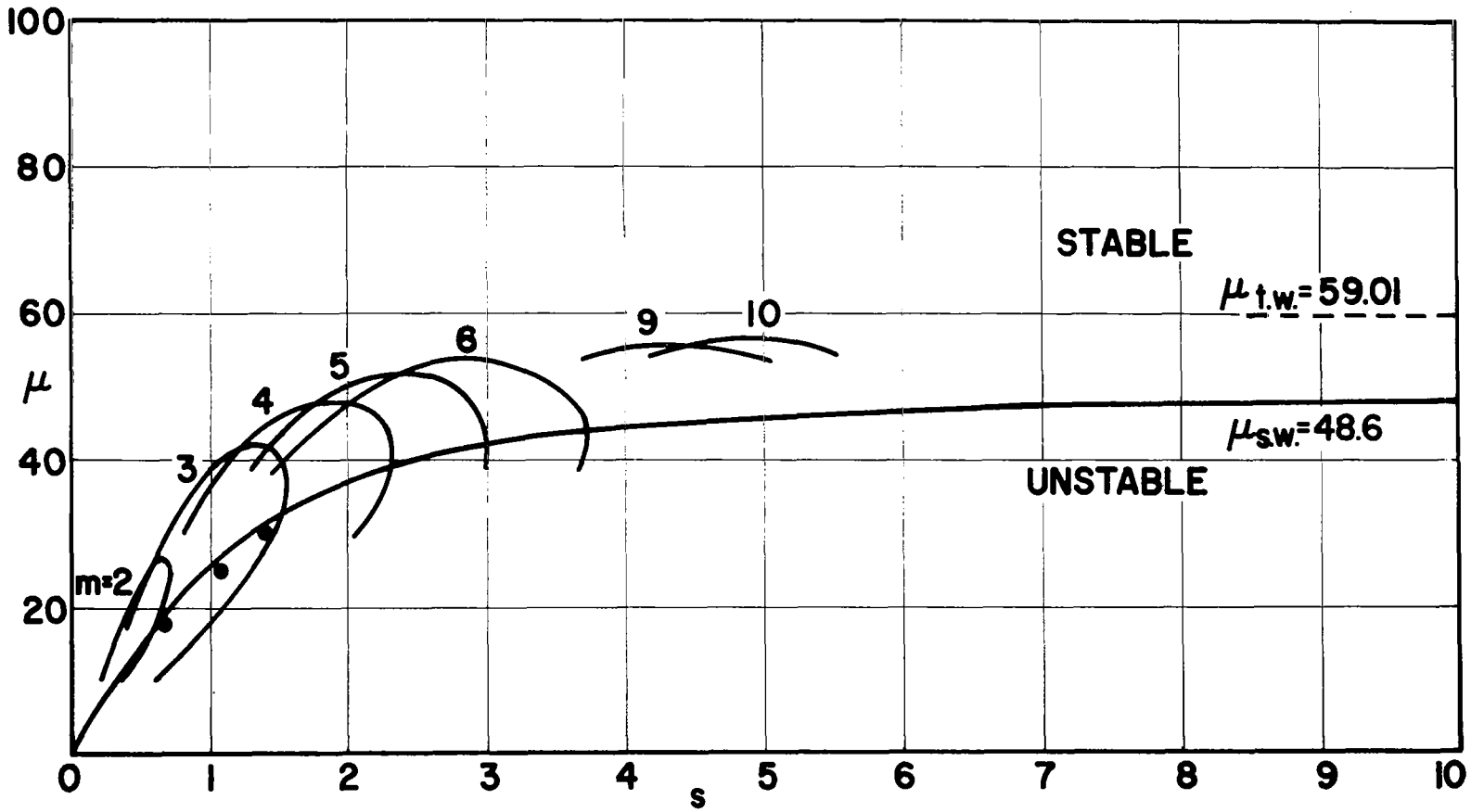

FIGURE 6c. DESIGN FLUTTER BOUNDARY (μ versus s); M = 1.35, η = 476.52, g = 0.01

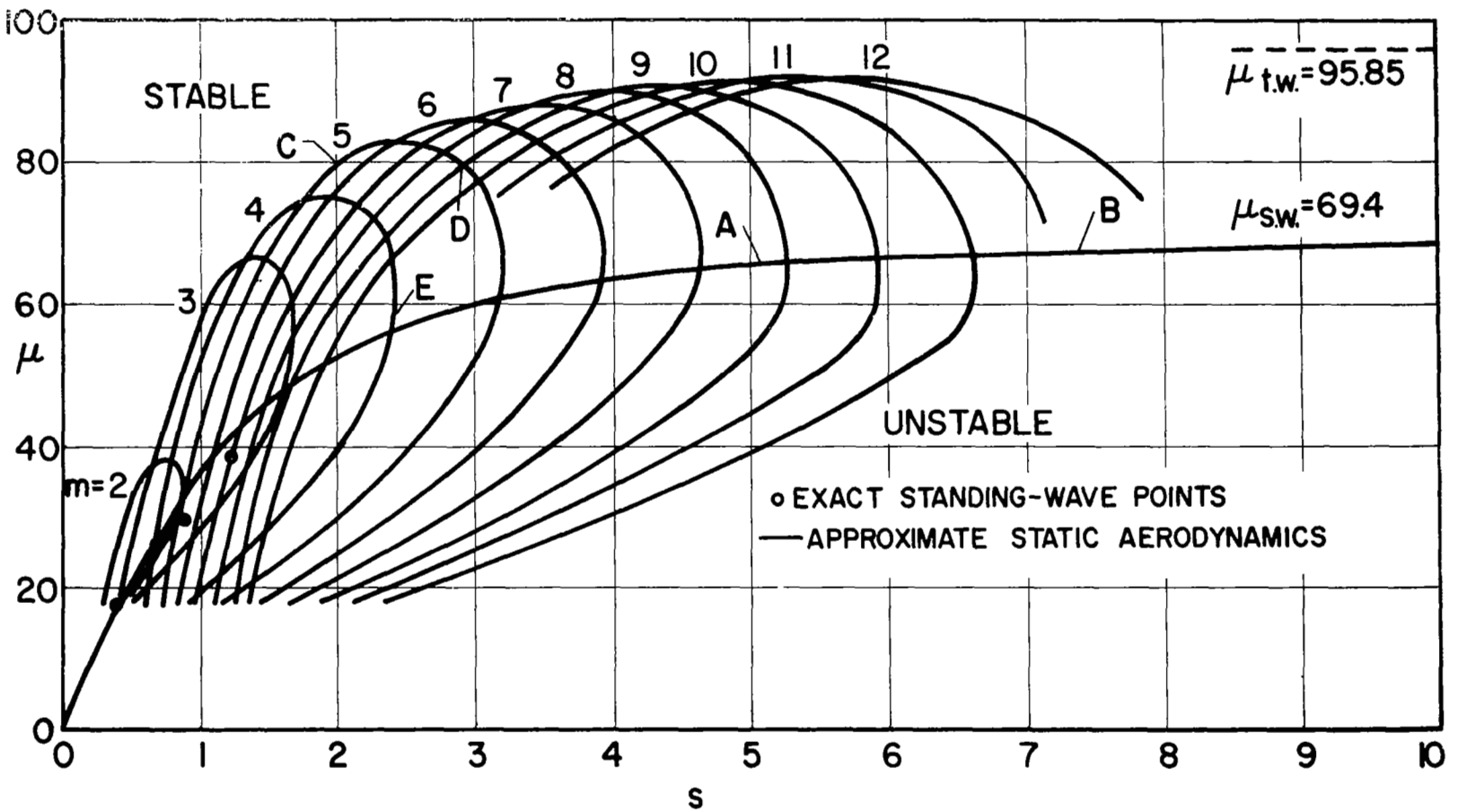

FIGURE 6d. DESIGN FLUTTER BOUNDARY (μ versus s); M = 1.35 , η = 810.0 , g = 0.01

A comparison of the traveling-wave branches in Figs. 6a, b, c, and d shows that the largest mass ratios to prevent flutter are required at the highest altitude (largest η). However, if we convert to thickness, following Appendix C, we find that the largest thickness is required at low altitude. The conversion to thickness is given in Table 2 for aluminum panels and $s = 1, 2, \infty$.

TABLE 2. THICKNESS REQUIRED FOR STABILITY AT M = 1.35 AND DIFFERENT ALTITUDES

	s = 1		s = 2		s = ∞	
η	μ	τ	μ	τ	μ	τ
190.8	17.6	.00584	22.0	.00730	26.4	.00875
331.0	28.5	.00511	36.0	.00645	42.6	.00765
476.5	39.0	.00479	50.0	.00614	59.0	.00724
809.8	58.0	.00421	80.0	.00581	95.9	.00696

The traveling-wave branch is the critical flutter boundary for all of the results in Fig. 6. It is of interest, however, to discuss the standing-wave branch. The small circles in Fig. 6 are standing-wave flutter points calculated with the exact theory for $g = .01$. They are points of coalescence of branches 1 and 2 in the k-s plane. The solid curve in each part of Fig. 6 is the result obtained with static aerodynamic theory for $g = 0$. The exact results are very close to, and slightly below, the static-theory curve. This result suggests that static-aerodynamic theory is adequate to predict the standing-wave branch of the flutter boundary even for relatively low Mach number. A similar and stronger point of view is expressed by Bohon and Dixon (Ref. 23). They give theoretical and experimental evidence to support the claim that the standing-wave branch (calculated with static aerodynamic theory) is the critical flutter branch even at Mach numbers as low as 1.3 when the length-to-width ratio is greater than unity. Results of the present study (see Fig. 6a) support this view for sea level conditions (small values

of $\bar{\eta}$). At higher altitude and low Mach number, there is a considerable difference between the standing- and traveling-wave boundaries (see Fig. 6d) and the latter is the critical branch.

The results presented in Fig. 6 also indicate that structural damping has a stabilizing effect on the standing-wave branch. Finally, we remark that the asymptote $\mu_{s.w.}$ of each standing-wave branch is given by the simple limit result (3.21).

The standing- and traveling-wave branches differ in several fundamental respects. First, the reduced frequencies are much smaller on the standing-wave branch - in particular, at higher altitude. Typical results are given in Table 3 for $s = \infty$.

TABLE 3. REDUCED FREQUENCIES FOR STANDING- AND TRAVELING-WAVE BRANCHES
($M = 1.35$, $s = \infty$)

η	k S-wave	k T-wave
190.8	0.234	0.987
331.0	0.198	1.078
476.5	0.173	1.129
809.8	0.147	1.192

Second, the mode shapes are vastly different. In Fig. 7, the standing-wave mode shapes are given for the two points A, B in Fig. 6d. The deflection is concentrated strongly near the trailing edge and has a very long wave length for large s . The traveling-wave mode shapes are shown in Fig. 8 for points C, D, E in Fig. 6d. The deflection is of much shorter wave length (order of the panel width) and is distributed over the panel length with only a slight concentration at the trailing edge. The mode shape at point C, which is a critical flutter point, is almost a pure sine wave. It illustrates why the traveling-wave flutter branch is often characterized as "single-degree-of-freedom-flutter" in the low supersonic regime.

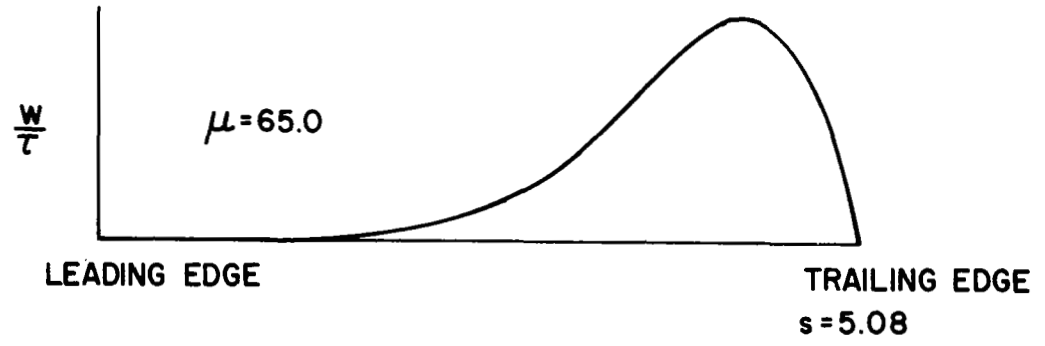

(a) Mode Shape at Point A in Fig. 6d

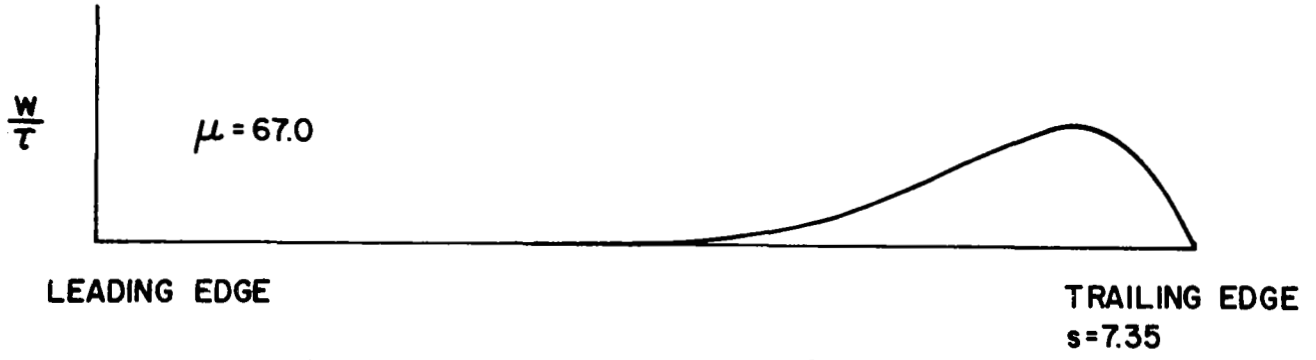

(b) Mode Shape at Point B in Fig. 6d

FIGURE 7. TYPICAL MODE SHAPES ON THE STANDING-WAVE FLUTTER BRANCH; $M = 1.35$, $\eta = 810.0$, $g = 0$

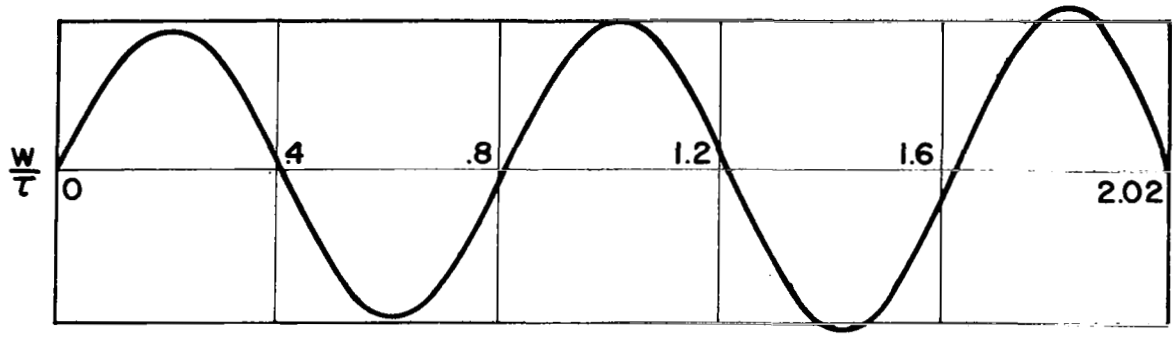

(a) Mode Shape at Point C in Fig. 6d

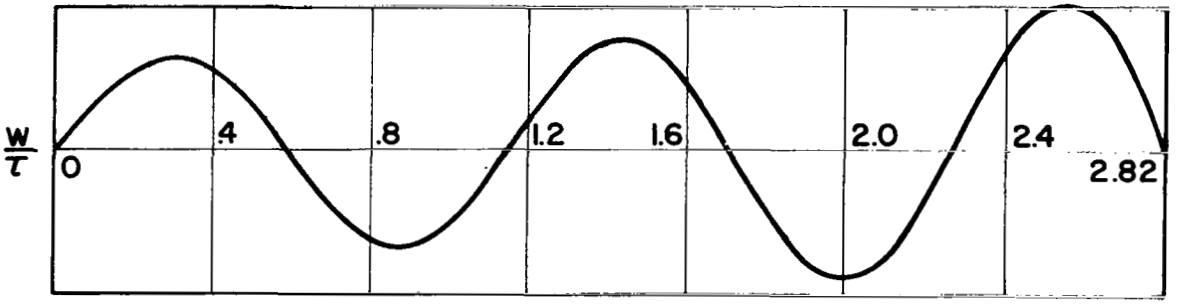

(b) Mode Shape at Point D in Fig. 6d

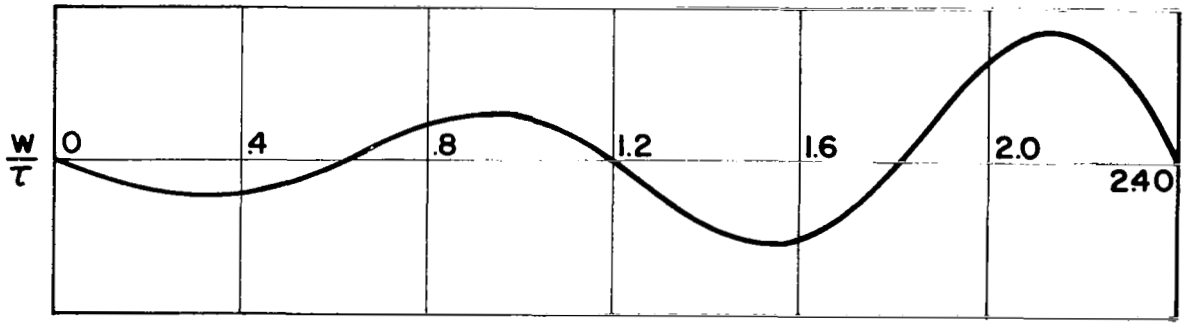

(c) Mode Shape at Point E in Fig. 6d

FIGURE 8. TYPICAL MODE SHAPES ON THE TRAVELING-WAVE FLUTTER BRANCH; $M = 1.35$, $\eta = 810.0$, $g = 0.01$

Maximum	Location
$w/\tau = .446$	$x = 1.26$
$s_x = 223$	$= 1.30$
$s_y = 94.5$	$= 1.26$

All maxima occur near the trailing edge ($s = 1.44$).

To use the dimensionless data to calculate stress, we proceed as follows. Suppose the panel is aluminum. From Fig. C-1 in Appendix C, we first convert the flutter μ into thickness for $\eta = 300$. We obtain

$$\tau = \frac{\mu}{2200}\left(\frac{\rho_\infty}{\rho_{\infty_0}}\right)$$

$$= \frac{28.7}{2200}\ (.445)$$

$$= .0058$$

Then from (1.21)

$$\sigma_{x\ max} = \frac{E\tau^2}{12(1 - \nu^2)}(s_x)_{max}$$

and for $E = 10^7$ psi and $\nu = .318$, we have

$$\sigma_{x\ max} = \frac{10^7(.0058)^2(223)}{12(1 - (.318)^2)}$$

$$= \underline{7110\ psi}$$

$$\sigma_{y\ max} = \underline{3020\ psi}$$

The conversion to stress for any panel material is equally straightforward.

The second example is for the following conditions:

$M = 1.35$	$g = .01$
$\eta = 260$	$r_{y_1} = 0$
$\mu = 18.8$	$r_{x_1} = 0,\ 100$

The mode shapes for a semi-infinite panel are shown in Fig. 9 for $M = 1.3$ and two different altitudes. At low altitude (Fig. 9b) the incident traveling wave is a pure sine wave to within about 5 panel widths of the trailing edge, where it grows to approximately twice the amplitude of the incident wave. At altitude (Fig. 9a) the incident wave is affected much sooner by the trailing edge, i.e., at about 10 panel widths. Then, the amplitude decays slightly before it grows again to twice the incident wave amplitude.

C. Sensitivity of Traveling-Wave Flutter to Structural Damping

We have seen that structural damping has a small stabilizing effect on the standing-wave flutter branch; also, for $M = 1.35$ and smaller, it has a slightly stabilizing effect on the traveling-wave branch. For larger Mach numbers, structural damping has a much larger stabilizing effect which we want to illustrate here.

The effect of structural damping is best illustrated with the weak asymptotic results presented in Section IIID. Referring to Fig. 4, the branches for which the real part of the flutter determinant, D_R, is zero are well approximated by (3.19a). The locus of points where $D_I = 0$ is approximated by (3.19b) (dashed line in Fig. 4). The accuracy of the latter curve is not as good as that of the real branches but is satisfactory for larger values of s. We therefore use (3.19) to demonstrate the effect of g on the traveling-wave flutter branch for large M.

For higher Mach number, the traveling wave flutter branch is typically like that in Fig. 14 in Section VF. The standing-wave branch is critical up to some value of s where flutter then becomes of the traveling-wave type. The minimum value of s where traveling-wave flutter can occur is approximated by the weak asymptotic formulae (3.19). The following typical result is obtained.

For $M = 2$ at sea level ($\eta = 147$) and $\mu = 60$, the minimum value of s for traveling-wave flutter is about 14

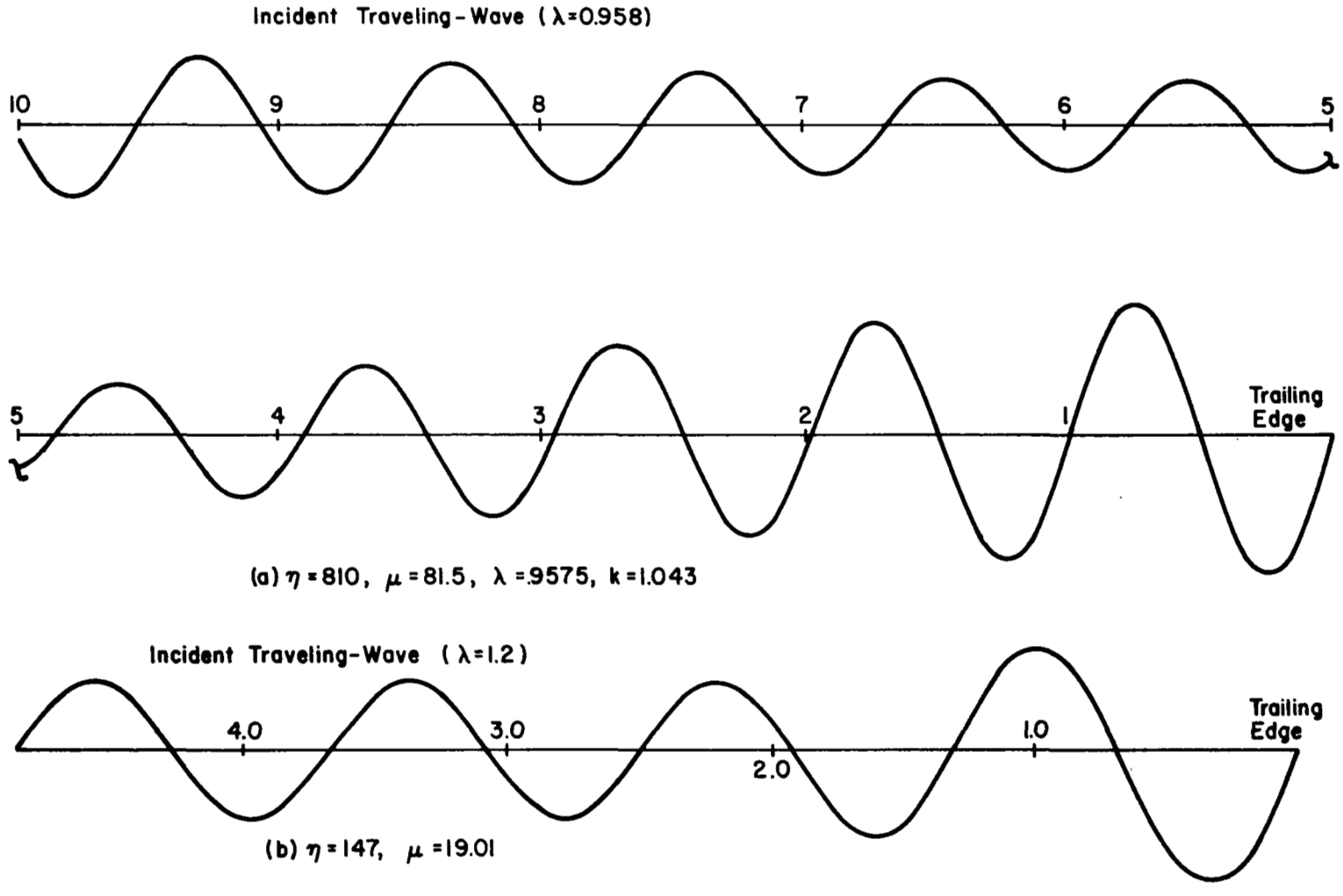

FIGURE 9. MODE SHAPES FOR A SEMI-INFINITE PANEL; M = 1.3 , ε = 0

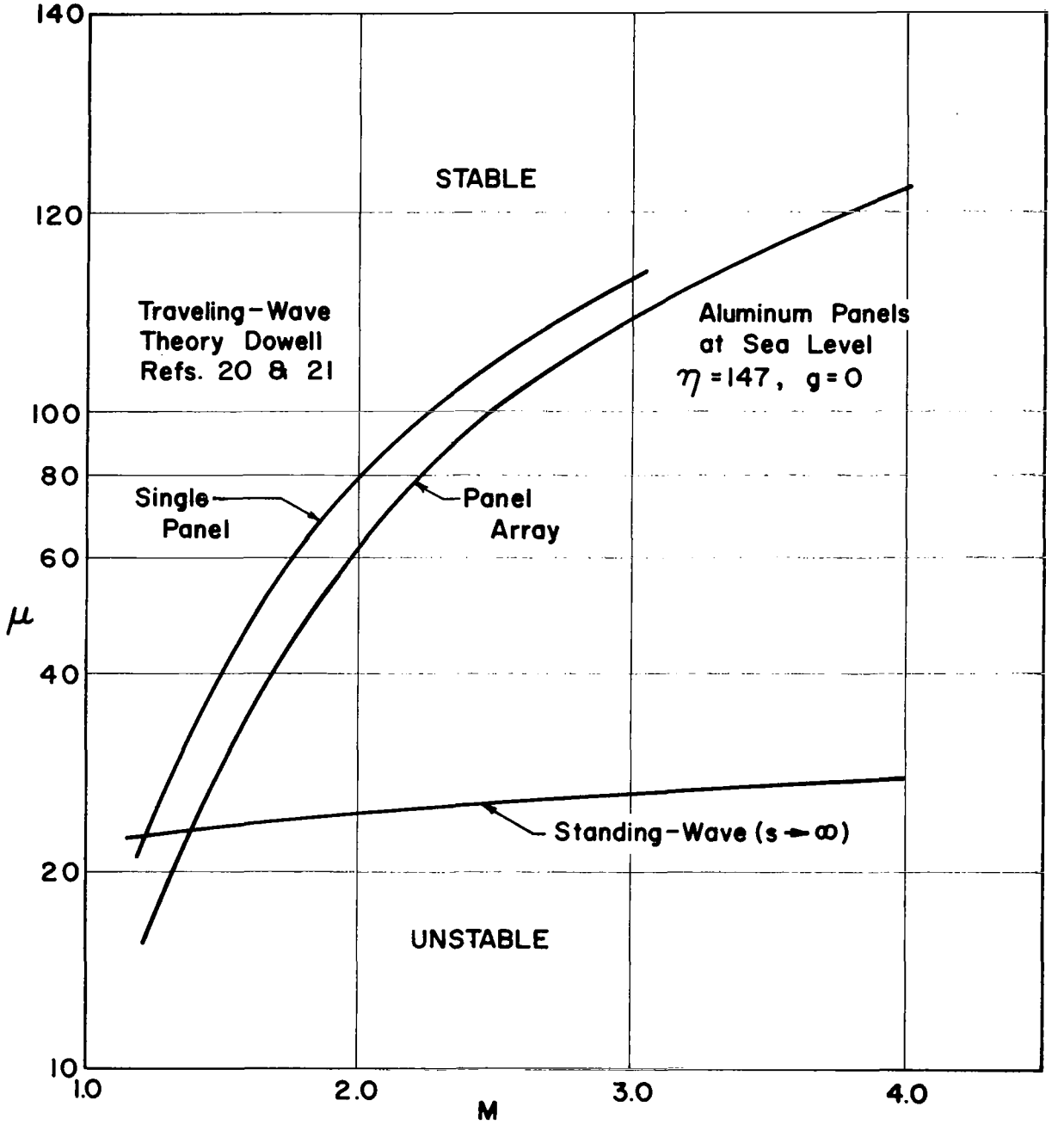

FIGURE 16. COMPARISON OF RESULTS FOR A SINGLE PANEL AND A PANEL ARRAY

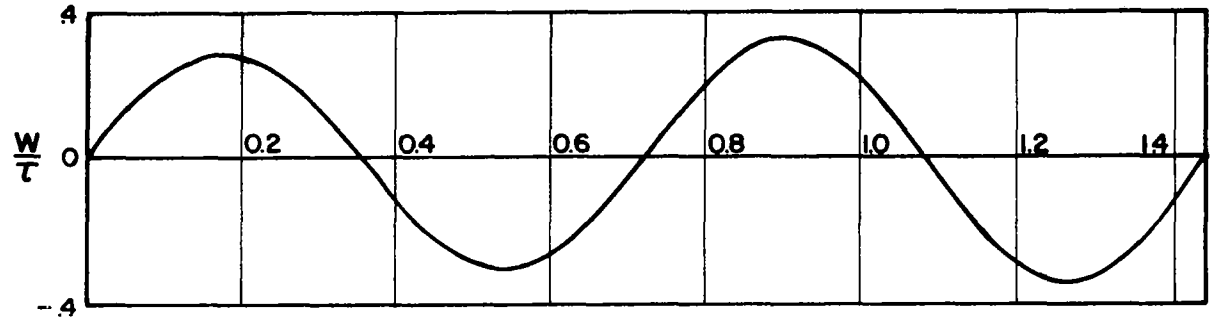

(a) Deflection Mode

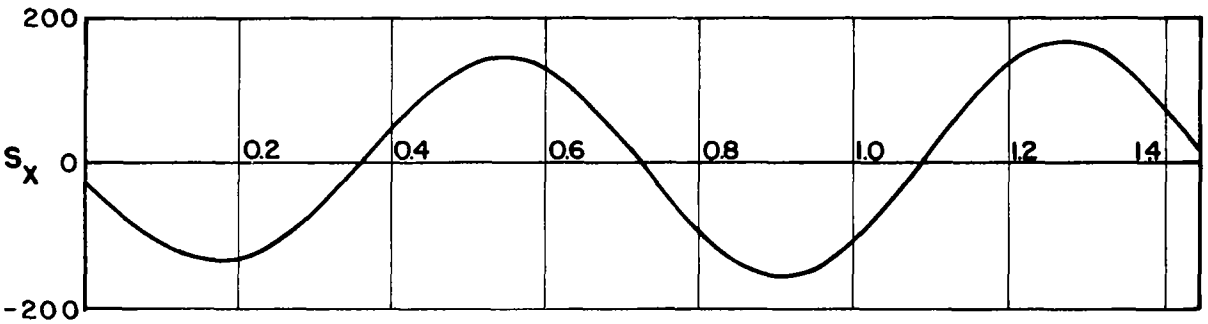

(b) Chordwise Stress Mode

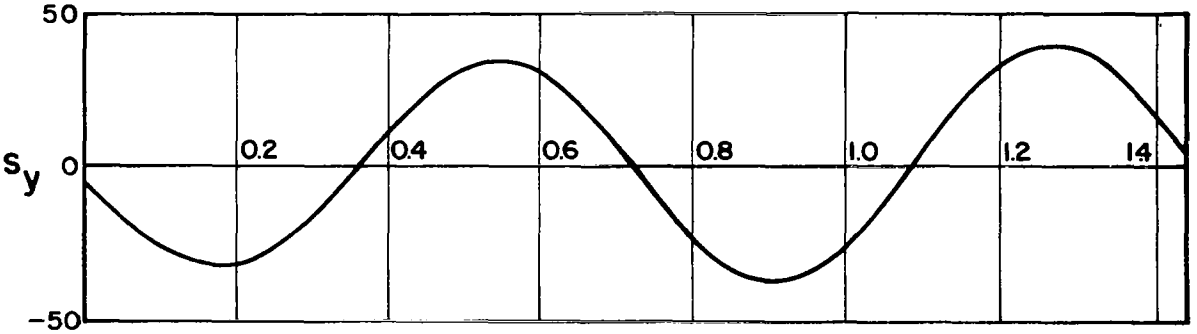

(c) Spanwise Stress Mode

FIGURE 11. DEFLECTION AND NONLINEAR STRESS MODE SHAPES; $M = 1.35$, $\eta = 300$, $\mu = 28.7$, $g = 0.01$, $r_{x_1} = 10$, $r_{y_1} = 0$

We compare the critical flutter point for $r_{x_1} = 0$ and 100. For $r_{x_1} = 0$, the critical flutter point is on branch 3 with $k = 2.273$ and $s = 0.935$. The stress level is zero. When $r_{x_1} = 100$, the critical point is on branch 5 with $k = 2.18$ and $s = 1.74$. The increase in s is a measure of the stabilizing effect of the nonlinear membrane stress.

The maximum deflection and stress for the case with $r_{x_1} = 100$ are as follows:

Maximum	Location
$w/\tau = 2.66$	$x = 1.65$
$s_x = 1705$	$= 1.70$
$s_y = 739$	$= 1.70$

Again, the maxima are near the trailing edge. The calculated stress levels in an aluminum panel are:

$$\sigma_x \quad 31{,}900 \text{ psi}$$
$$\sigma_y = 13{,}800 \text{ psi}$$

The stress in the first example is essentially below the fatigue limit for aluminum and so can be termed a weak flutter point. For the stress in the second example, a fatigue life of approximately 100,000 cycles can be expected (see Ref. 24). For an aircraft panel, such flutter cannot be tolerated. However, for a one-shot missile application, such a stress level may be satisfactory when the number of cycles is quite small. Further discussion of the fatigue life of Saturn V panels is given in the following section.

F. Flutter Boundaries for a Saturn V Operational Trajectory

We conclude our investigation with some results for aluminum panels on a typical Saturn V operational trajectory. The pertinent trajectory data (supplied by Marshall Space Flight Center) are given in Fig. 12 and Table 4. The vehicle goes

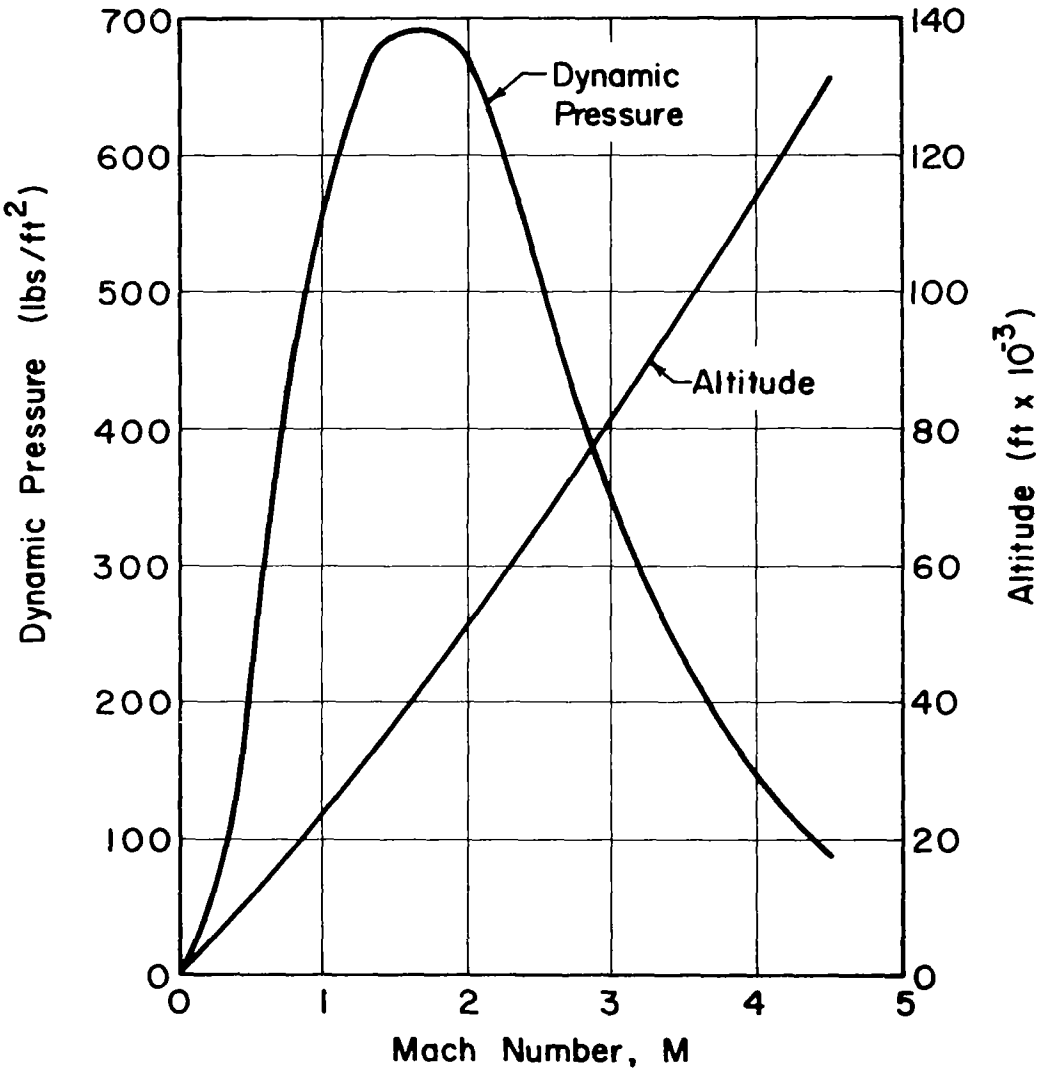

FIGURE 12. SATURN V AS-507 OPERATIONAL FLIGHT TRAJECTORY (SUPPLIED BY MSFC)

TABLE 4. DATA FOR SATURN V TRAJECTORY

Altitude ft	M	Dynamic Pressure lb/ft^2	ρ/ρ_o	p/p_o	a/a_o	η/η_o	Aluminum η
25,000	1.00	557	.4486	.3716	.911	2.03	275
30,000	1.19	625	.3747	.2975	.891	2.38	327
35,000	1.37	677	.3106	.2359	.871	2.80	384
40,000	1.55	690	.2471	.1858	.868	3.51	482
45,000	1.75	690	.1945	.1462	.868	4.46	612
50,000	1.93	680	.1531	.1151	.868	5.66	778
55,000	2.11	635	.1206	.0907	.868	7.20	988
60,000	2.30	583	.0942	.0714	.868	9.20	1260

through $M = 1$ at an altitude of 25,000 ft and reaches maximum dynamic pressure at 40,000 ft and $M = 1.55$.

Complete design flutter boundaries (μ versus s) were calculated at two points on the trajectory, $M = 1.37$, $\eta = 384$ and $M = 1.55$, $\eta = 482$. The results are shown in Figs. 13 and 14 . The results in Fig. 13 are very similar to those presented in Section IVB . The traveling-wave branch is the critical flutter branch for all s . Also, both branches tend asymptotically to the respective limits $\mu_{t.w.}$ and $\mu_{s.w.}$ for large s . The results in Fig. 14 are typical of the type of flutter boundaries obtained for higher Mach numbers. The standing-wave branch is the critical flutter branch up to $s = 3.1$. Then, the traveling-wave branch becomes critical with a jump in the mass ratio or thickness required for stability; also, there is a jump in the frequency. The asymptote of the traveling-wave branch is considerably less than $\mu_{t.w.}$ due to structural damping. As was pointed out in Section IVC , this sensitivity to small values of g is typical at higher Mach numbers.

Finally, we give a design flutter boundary (thickness-to-width ratio versus altitude) for aluminum panels on the Saturn V - S-IVB forward skirt. The material properties are:

$$E = 10.3 \times 10^6 \text{ psi}$$
$$\nu = 0.33$$
$$\rho_s = 5.36 \text{ slugs/ft}^3$$
$$a_s = 18{,}450 \text{ ft/sec} .$$

Curves of τ versus altitude are given in Fig. 15 for two length-to-width ratios, $s = 2$ and $s = 4.48$. The latter case corresponds to an actual panel used on the forward skirt of the S-IVB stage. The flutter boundary obtained with the traveling-wave theory is also shown for comparison.

For fixed length-to-width ratio, the critical flutter boundary is the dome-shaped region for small Mach number and the standing-wave branch for larger Mach number. This is a familiar

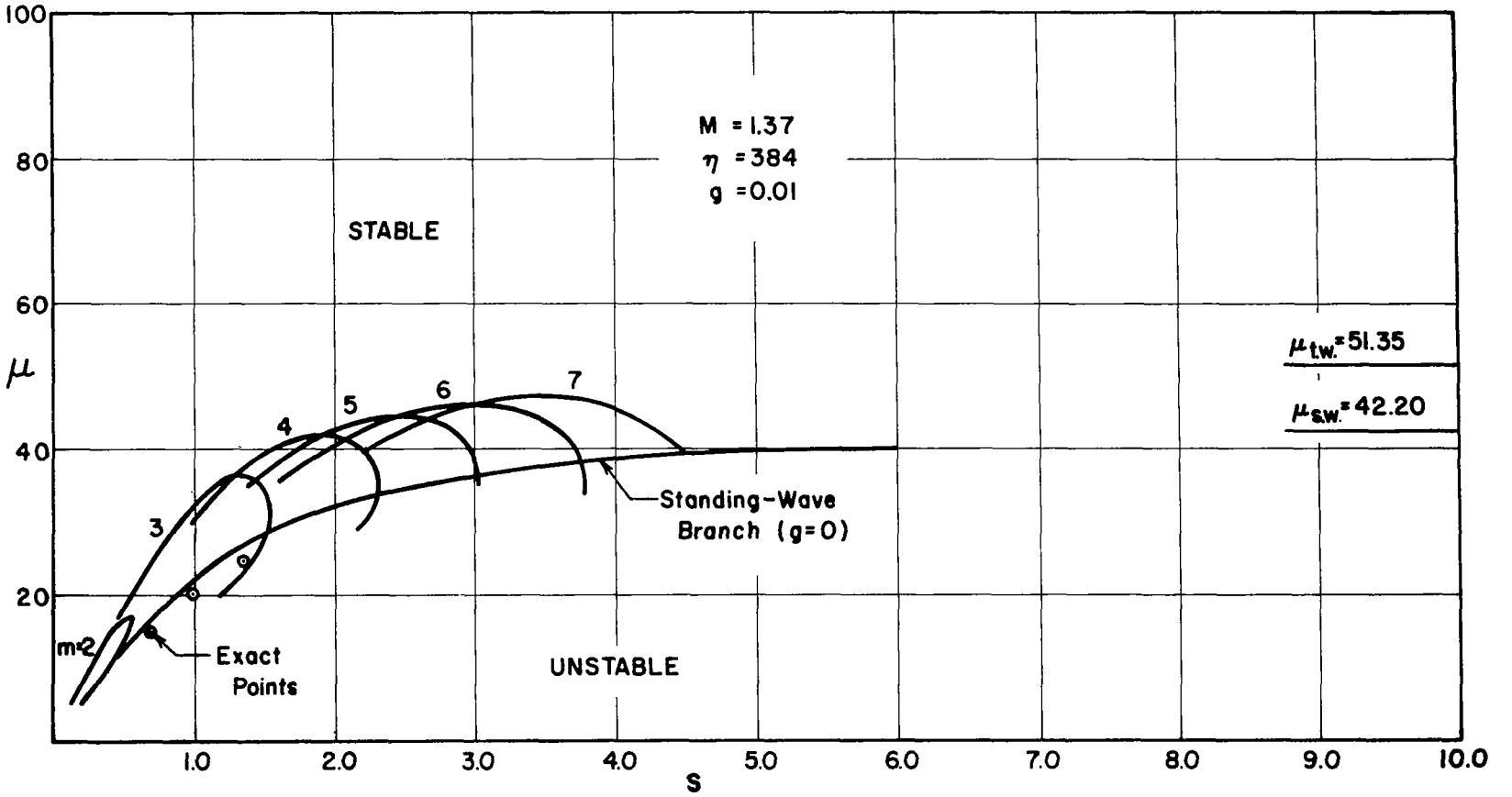

FIGURE 13. DESIGN FLUTTER BOUNDARY (μ versus s) FOR A POINT ON A SATURN V TRAJECTORY; M = 1.37 , η = 384 , g = 0.01

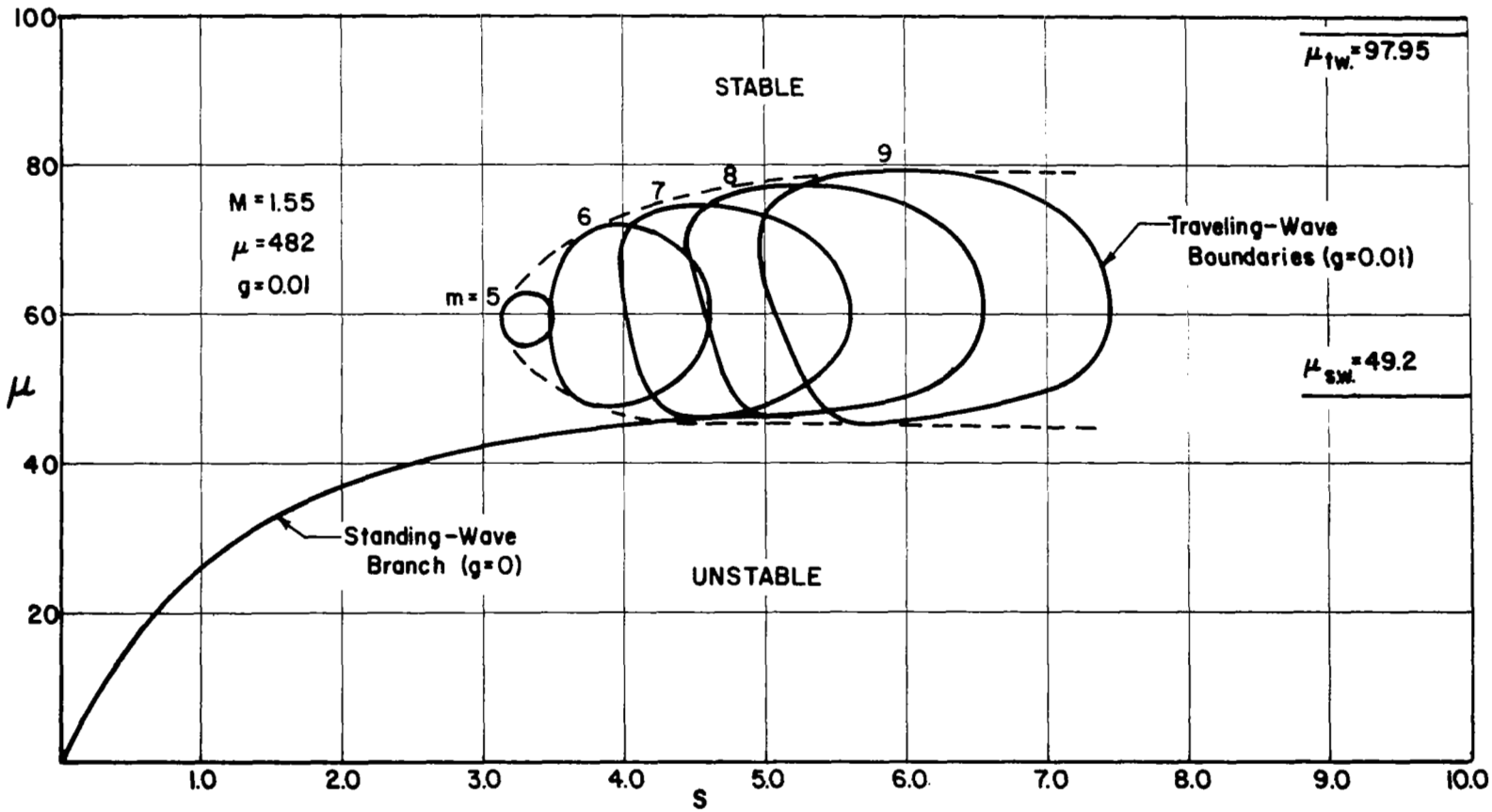

FIGURE 14. DESIGN FLUTTER BOUNDARY (μ versus s) FOR A POINT ON A SATURN V TRAJECTORY; M = 1.55 , η = 482 , g = 0.01

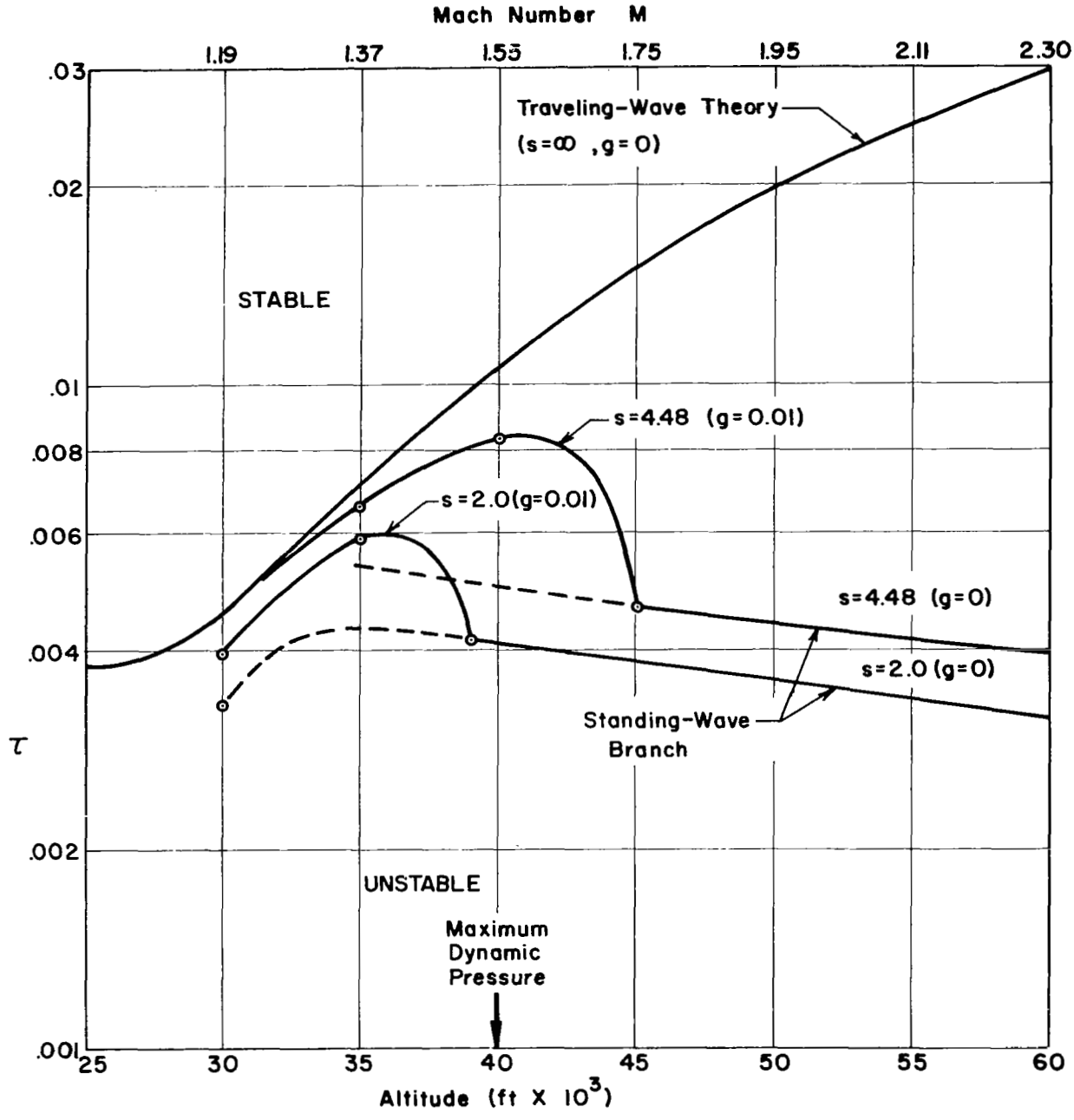

FIGURE 15. DESIGN FLUTTER BOUNDARY (τ versus Altitude) FOR ALUMINUM PANELS ON A SATURN V TRAJECTORY

type of flutter boundary (see e.g., Refs. 12, 25, 26) that shows quite clearly the increased thickness requirements in the low Mach number range. The present results provide several insights into this familiar phenomenon. First of all, they show the sharp transition from flutter of the traveling-wave type to flutter of the standing-wave type. The transition Mach number depends strongly on the length-to-width ratio and the level of structural damping. As the length-to-width ratio is increased, the critical flutter boundary coincides with the simple traveling-wave theory to somewhat higher Mach number. However, the presence of any small amount of damping eventually causes the flutter boundary to make the transition from the traveling-wave branch to the standing-wave branch. (Compare with Fig. 4, Ref. 26) The rapid increase in thickness requirements with s points to the fact that long narrow panels should be avoided in design situations if at all possibile.

One of the panels on the S-IVB forward skirt has a length-to-width ratio of 4.48 and a thickness-to-width ratio of 0.0048. Flutter was detected in flight (Ref. 27). From the durve for $s = 4.48$ in Fig. 15 , we predict that flutter should set in just above 30,000 ft and subside at 45,000 ft . The theory indicates that the flutter is of the traveling-wave type with 7 or 8 half waves in the mode shape. Also, flutter occurs in the region of maximum dynamic pressure.

Some remarks on the fatigue life of the panel are in order. The vehicle traverses the 15,000 ft region of panel flutter at an average velocity of about 1500 ft/sec so that the actual time of flutter is, at most, 10 sec . The flutter frequency is approximately 450 cps . Thus, the panel undergoes approximately 4500 cycles of stress reversal. The stress level calculated in the second of the two examples in Section IV-B was 31,900 psi . The fatigue life at this level is 100,000 cycles so that flutter would not be destructive. We note, in fact, that a stress level of 45,000 psi is tolerable without failure with only 5000 cycles (Ref. 24). The relatively short duration of flutter in a

Saturn V flight points to the need for a reasonable estimate of the stress level so that fatigue may be used as a criterion for design.

V. SUMMARY OF CONCLUSIONS

We have presented a general theory for calculating flutter boundaries and making stress estimates for an infinite spanwise array of panels. The principal conclusions of the study are:

1. Calculations of flutter points and mode shapes with the exact Zeydel method are in complete agreement with results obtained with the Galerkin method when the latter are converged.

2. The Zeydel method yields a flutter boundary for all length-to-width ratios, but is particularly suited to low-aspect ratio panels where modal analyses are difficult, if not impossible, to apply.

3. For fixed panel width, the thickness required to present flutter increases with length-to-width ratio, s, and approaches a limiting value as $s \to \infty$.

4. The flutter thickness is largest at low altitudes.

5. Two distinct flutter branches are predicted by the exact theory. The first branch occurs at low reduced frequency (order of a few tenths) and agrees with results based on the simple static aerodynamic theory. We call it the standing-wave branch. The other branch is obtained at higher reduced frequency (order unity) and tends asymptotically to results based on traveling-wave theory as $s \to \infty$, providing $g = 0$. We call it the traveling-wave branch.

6. At low Mach number, the traveling-wave branch is the critical flutter branch and gives the well-known dome-shaped flutter boundary in the low supersonic regime. At higher Mach number and finite s, the standing-wave branch is critical.

7. The Mach number for transition from traveling-wave flutter to standing-wave flutter is very sensitive to structural damping and the length-to-width ratio. The dome-shaped flutter boundary extends to higher Mach number when s is large.

8. Small values of structural damping are highly stabilizing and essentially eliminate the traveling-wave flutter branch at higher Mach number.

9. The flutter thickness for an array of panels is smaller than that for a single panel when the Mach number is moderately low and s is large.

10. Two example stress calculations are given. The maximum stress occurs near the trailing edge and close to the point of maximum deflection.

11. Design flutter boundaries for aluminum panels on a typical Saturn V operational trajectory are given. Flutter is predicted in the region of maximum dynamic pressure for a panel on the forward skirt of the S-IVB stage in agreement with flight data. Failure of these panels is not likely because of the relatively low number of stress reversals in flying through the critical flutter region.

APPENDIX A

Mode Shape for a Partially Clamped Beam

Here we consider the problem of calculating the eigenvalues, mode shapes and certain integrals of the mode shapes of a partially clamped beam. The problem is stated mathematically as follows:

$$\frac{d^4 g}{dy^4} - \beta^4 g = 0$$

$$g(0) = g(1) = 0$$

$$\epsilon_c g'(0) - \epsilon_p g''(0) = 0$$

$$\epsilon_c g'(1) + \epsilon_p g''(1) = 0 \qquad \text{(A.1)}$$

where ϵ_p , ϵ_c vary between zero and one and give the relative degree of end fixity.

The general solution of the beam equation can be expressed in the form

$$g(y) = A \sin(\beta y - \phi) + Be^{-\beta y} + Ce^{-\beta(1-y)} \qquad \text{(A.2)}$$

Now apply the boundary conditions $g(0) = g(1) = 0$. We obtain a pair of equations for B and C :

$$\begin{bmatrix} 1 & e^{-\beta} \\ e^{-\beta} & 1 \end{bmatrix} \begin{Bmatrix} B \\ C \end{Bmatrix} = - A \begin{Bmatrix} -\sin\phi \\ \sin(\beta - \phi) \end{Bmatrix} \qquad \text{(A.3)}$$

To calculate B and C we neglect terms of order $e^{-2\beta}$ compared to unity. This is justified on the grounds that the smallest eigenvalue of a pinned-pinned beam is π and of a clamped-clamped beam is 4.73. Thus

$$e^{-2\beta} < .002 \quad \text{pinned-pinned}$$

$$< .0001 \quad \text{clamped-clamped} \qquad \text{(A.4)}$$

For arbitrary values of ϵ_p and ϵ_c we expect the error, therefore, to be correspondingly small. This approximation is used throughout the subsequent discussion.

With the foregoing remark we calculate the solution of (A.3)

$$B = A\left[\sin\phi + e^{-\beta}\sin(\beta - \phi)\right]$$

$$C = -A\left[e^{-\beta}\sin\phi + \sin(\beta - \phi)\right] \qquad (A.5)$$

and write the general solution in the form

$$g(y) = A\left\{\sin(\beta y - \phi) + \left[\sin\phi + e^{-\beta}\sin(\beta - \phi)\right]e^{-\beta y} - \left[e^{-\beta}\sin\phi + \sin(\beta - \phi)\right]e^{-\beta(1-y)}\right\} \qquad (A.6)$$

It remains to determine the phase factor ϕ and the eigenvalues β.

Application of the remaining boundary conditions yields the following pair of equations for ϕ and β:

$$\begin{bmatrix} \epsilon_c(1 - 2e^{-\beta}\sin\beta) & -(\epsilon_c + 2\epsilon_p\beta - 2\epsilon_c e^{-\beta}\cos\beta) \\ \epsilon_c\cos\beta & (2\epsilon_p\beta + \epsilon_c)\cos\beta \\ -(2\epsilon_p\beta + \epsilon_c)\sin\beta & +\epsilon_c\sin\beta - 2\epsilon_c e^{-\beta} \end{bmatrix} \begin{Bmatrix} \cos\phi \\ \\ \sin\phi \end{Bmatrix} = 0 \qquad (A.7)$$

Since $\cos\phi$ and $\sin\phi$ cannot be zero simultaneously, the determinant of the coefficient matrix must vanish. Thus, we obtain the characteristic equation for the eigenvalues,

$$\boxed{\epsilon_c(\epsilon_c + 2\epsilon_p\beta)\cos\beta - 2\epsilon_p\beta(\epsilon_c + \epsilon_p\beta)\sin\beta = 2\epsilon_c{}^2 e^{-\beta}} \qquad (A.8)$$

The phase factor ϕ is calculated from either of the equations in (A.7). Thus we have

$$\tan \phi = \frac{\epsilon_c \left(1 - 2e^{-\beta} \sin \beta\right)}{\epsilon_c + 2\epsilon_p \beta - 2\epsilon_c e^{-\beta} \cos \beta} \qquad -\frac{\pi}{2} < \phi < \frac{\pi}{2} \tag{A.9}$$

The mode shape corresponding to each eigenvalue is given by (A.6) with an appropriate choice of the normalization factor A.

Two familiar special cases are the following:

Pinned Edges

For this case we have $\epsilon_c = 0$ and $\epsilon_p = 1$. Thus we obtain from (A.8) and (A.9)

$$-2\epsilon_p{}^2\beta^2 \sin \beta = 0 \rightarrow \sin \beta = 0 \Rightarrow \beta = \bar{n}\pi \qquad \bar{n} = 1,2,\ldots$$

$$\tan \phi = 0 \rightarrow \phi = 0$$

$$g(y) = A \sin \bar{n}\pi y \qquad \bar{n} = 1,2,\ldots \tag{A.10}$$

Clamped Edges

For this case we have $\epsilon_c = 1$ and $\epsilon_p = 0$. Thus we have

$$\cos \beta = 2e^{-\beta} \qquad \tan \phi = 1 - 2e^{-\beta} \sin \beta \tag{A.11}$$

The solution for β and ϕ is

$$\beta_{\bar{n}} = \frac{2\bar{n} + 1}{2}\pi - 2(-1)^{\bar{n}} e^{-\frac{2\bar{n}+1}{2}\pi}$$

$$\phi_{\bar{n}} = \frac{\pi}{4} - 2(-1)^{\bar{n}} e^{-\frac{2\bar{n}+1}{2}\pi} \qquad \bar{n} = 1,2,\ldots \tag{A.12}$$

and for the mode shape we use (A.6).

Integrals

It is next of interest to consider the following integrals of the mode shape

$$C_n = -\int_0^1 \frac{d^n g(y)}{dy^n} \cdot g(y)\, dy \tag{A.13}$$

We define C_o to be minus unity. This normalizes $g(y)$ and fixes the constant A in (A.6). Upon integration we find

$$A = \frac{\sqrt{2}}{\left[1 - 4e^{-\beta} \sin\phi \sin(\beta - \phi)\right]^{\frac{1}{2}}}$$

$$= \sqrt{2} \quad \text{pinned}$$

$$\cong \frac{\sqrt{2}}{1 - (-1)^{\bar{n}_e - \beta\bar{n}}} \quad \text{clamped} \tag{A.14}$$

Next consider the integral

$$C_1 = -\int_0^1 g(y) \frac{dg}{dy}\, dy \tag{A.15}$$

Now the mode shapes are either symmetric or antisymmetric about the center $y = 1/2$. Thus

$$g(y) = \pm\, g(1 - y) \qquad \begin{cases}\text{symmetric} \\ \text{antisymmetric}\end{cases} \tag{A.16}$$

In (A.15), we let $y = 1 - t$ so that

$$C_1 = \int_0^1 g(1 - t) \frac{d}{dt} g(1 - t)\, dt$$

$$= \int_0^1 g(t) \frac{d}{dt} g(t)\, dt$$

$$= -\, C_1 \tag{A.17}$$

We conclude that $C_1 = 0$ for all modes.

The integral C_2 has the following form

$$C_2 = \frac{A^2\beta^2}{2}\left\{1 - \frac{1}{\beta}\left[\sin\phi\,(\cos\phi + \sin\phi) + \sin(\beta-\phi)\Big(\cos(\beta-\phi) + \sin(\beta-\phi)\Big)\right] + 4\Big(1 - \frac{1}{\beta}\Big)\,e^{-\beta}\sin\phi\,\sin(\beta-\phi)\right\} \qquad (A.18)$$

where A is given by (A.14). For pinned and clamped edges we have

$$C_2 = (\bar{n}\pi)^2 \qquad \text{pinned}$$

$$= \frac{\beta_{\bar{n}}\left[\beta_{\bar{n}}\Big(1 + 2(-1)^{\bar{n}}e^{-\beta_{\bar{n}}}\Big) - 2\right]}{1 - 2(-1)^{\bar{n}}e^{-\beta_{\bar{n}}}} \qquad \text{clamped} \qquad (A.19)$$

The integral C_3 is zero by the same argument leading to C_1. For C_4 we use the differential equation to get

$$C_4 = -\int_0^1 \frac{d^4g}{dy^4}\,g\,dy = -\int_0^1 \beta^4 g^2\,dy$$

$$= -\beta_{\bar{n}}^4 \qquad (A.20)$$

APPENDIX B

Numerical Algorithm for $F_n(x)$

Here we give a procedure for evaluating each of the characteristic functions numerically. We have

$$F_n(x) = e^{p_n x}\left(A_n - B_n G_n(x)\right) \tag{B.1}$$

$$G_n(x) = \int_0^x e^{-(p_n+iKM)\xi} J_o(\Gamma\xi)d\xi \tag{B.2}$$

$$A_n = \frac{h(p_n)g(p_n)}{\Delta'(p_n)} \quad , \quad B_n = \frac{h(p_n)\ell(p_n)}{\Delta'(p_n)}$$

$$\bar{D}^+(p_n) = 0 \quad , \quad n = 1,2,3,4,5$$

$$\bar{D}^-(p_n) = 0 \quad , \quad n = 6,7,8,9,10$$

$$\bar{D}^{\pm}(p) = g(p) \pm \frac{\ell(p)}{h^{\frac{1}{2}}(p)} \tag{B.3}$$

To evaluate $F_n(x)$ we use an approximation of the Bessel function given by Luke (Ref.28) for small argument and the asymptotic expansion for large argument. Thus

$$J_o(t) = \frac{1}{q}\sum_{r=1}^{q} \cos \lambda_r t + 2J_{4q}(t) \qquad t < a$$

$$\lambda_r = \cos\left(\frac{2r-1}{4q}\pi\right)$$

$$= \sqrt{\frac{2}{\pi t}} \cos\left(t - \frac{\pi}{4}\right) \qquad t > a \tag{B.4}$$

where a is the crossover point. The error term in Luke's

approximation of J_o is proportional to $J_{4q}(t)$, and so decreases rapidly with increasing q for fixed t. For example, if $q = 10$, the approximation is accurate to four decimal places for $t \leq 24$. Since the asymptotic expansion is good to four decimal places for $t \geq 24$ we have a uniform approximation of $J_o(t)$ for all t. Also the approximation is most convenient for subsequent integrations that must be performed.

Because of the split range of the J_o approximation, there are two cases to consider in the evaluation of $F_n(x)$; i.e., $x < a/\Gamma$ and $x > a/\Gamma$:

Small Argument $(x < a/\Gamma)$

For $x < a/\Gamma$ we substitute the approximation of Luke into (B.2) to obtain

$$G_n(x) = \frac{1}{q} \sum_{r=1}^{q} \frac{1}{\Gamma\lambda_r} \cdot I\left(\frac{p_n + iKM}{\lambda_r \Gamma} \;,\; \lambda_r \Gamma x\right)$$

where

$$I(\alpha,x) = \int_0^x e^{-\alpha t} \cos t \, dt \qquad \text{(B.5)}$$

By straightforward evaluation, we get

$$I(\alpha,x) = \frac{\alpha(1 - e^{-\alpha x}) \cos x + e^{-\alpha x} \sin x}{\alpha^2 + 1}$$

$$a|\alpha \pm i| > \epsilon$$

$$= \frac{ix\left[1 - (\alpha - i)x\right] + 1 - e^{-\alpha x} \cos x}{\alpha + i\delta} + O\left(\frac{a\epsilon^2}{12}\right)$$

$$a|\alpha - i| \leq \epsilon$$

$$= \frac{-ix\left[1 - (\alpha + i)x\right] + 1 - e^{-\alpha x} \cos x}{\alpha - i\delta} + O\left(\frac{a\epsilon^2}{12}\right)$$

$$a|\alpha + i| \leq \epsilon$$

(B.6)

The second two formulae are needed when a root is near the line joining the two branch points.

Large Argument ($x > a/\Gamma$)

For $x > a/\Gamma$ the problem is slightly more complicated. The plan is to evaluate $G_n(x)$ for $\mathrm{Re}\ p_n > 0$ and extend the result to the left half plane by analytic continuation. We write

$$G_n(x) = \int_0^\infty e^{-(p_n+iKM)\xi} J_o(\Gamma\xi)d\xi - \overline{G}_n(x)$$

$$= h^{-\frac{1}{2}}(p_n) - \overline{G}_n(x) \qquad \text{(B.7)}$$

and so

$$F_n = 2A_n e^{p_n x} + \overline{F}_n(s) \qquad n = 1,2,3,4,5$$

$$= \overline{F}_n(s) \qquad n = 6,7,8,9,10 \qquad \text{(B.8)}$$

where

$$\overline{F}_n(s) = B_n e^{p_n x}\ \overline{G}_n(x)$$

$$\overline{G}_n(x) = \int_x^\infty e^{-(p_n+iKM)\xi} J_o(\Gamma\xi)d\xi \qquad \text{(B.9)}$$

To evaluate $\overline{G}_n(x)$ we substitute the asymptotic approximation for J_o into (B.9). We get

$$\overline{G}_n(x) = \sqrt{\frac{2}{\pi}} \cdot \frac{1}{\Gamma} \int_{\Gamma x}^\infty e^{-\alpha t} \cos\,(t - \pi/4)\, \frac{dt}{\sqrt{t}}$$

$$\alpha = \frac{(p_n + iKM)}{\Gamma} \qquad \text{(B.10)}$$

This integral is easily evaluated in terms of the complementary error function. The final result is

$$\bar{G}_n(x) = \frac{1}{\sqrt{2\Gamma}} \left\{ e^{-i\frac{\pi}{4}} \frac{\operatorname{erf}\sqrt{[p_n+i(KM-\Gamma)]x}}{\sqrt{p_n+i(KM-\Gamma)}} + e^{i\frac{\pi}{4}} \frac{\operatorname{erfc}\sqrt{[p_n+i(KM+\Gamma]x}}{\sqrt{p_n+i(KM+\Gamma)}} \right\} \tag{B.11}$$

where

$$\operatorname{erfc} z = \frac{2}{\sqrt{\pi}} \int_z^\infty e^{-t^2}\, dt \tag{B.12}$$

The result (B.11) is an analytic function of p_n, except at the two branch points, and is a valid representation of $\bar{G}_n(x)$ in the right half plane $\operatorname{Re} p_n > 0$. By analytic continuation we conclude that (B.11) is valid for all p_n in the complex plane.

To evaluate **erfc z** for complex argument, the following formulae are useful (Ref.29)

$$\operatorname{erfc} z = 1 - \operatorname{erf} z$$

$$\operatorname{erf}(x + iy) = \operatorname{erf} x + \frac{e^{-x^2}}{2\pi x}\left[(1 - \cos 2xy) + i \sin 2xy\right]$$

$$+ \frac{2}{\pi} e^{-x^2} \sum_{n=1}^{\infty} \frac{e^{-\frac{1}{4}n^2}}{n^2+4x^2}\left[f_n(x,y) + i g_n(x,y)\right] + \epsilon(x,y) \tag{B.13}$$

where

$$f_n(x,y) = 2x - 2x \cosh ny \cos 2xy + n \sinh ny \sin 2xy$$

$$g_n(x,y) = 2x \cosh ny \sin 2xy + n \sinh ny \cos 2xy$$

$$|\epsilon(x,y)| \cong 10^{-16} |\operatorname{erf}(x + iy)| \tag{B.14}$$

$$\operatorname{erfc} z \sim \frac{e^{-z^2}}{\sqrt{\pi}\, z}\left(1 + \frac{1}{2z^2} + 0\left(\frac{1}{z^4}\right)\right) \tag{B.15}$$

$$z \to \infty$$

$$|\arg z| < 3\frac{\pi}{4}$$

In conclusion we give the following formulae for A_n and B_n that are easily derived from their basic definitions:

$$B_n = \frac{\ell(p_n)}{g(p_n)} \; A_n$$

$$A_n = g'(p_n) + g(p_n)\left[\frac{\ell'(p_n)}{\ell(p_n)} - \frac{h'(p_n)}{2h(p_n)}\right] \qquad \text{(B.16)}$$

$$g(p_n) = p_n^4 - Ap_n^2 + B \quad , \quad g'(p_n) = 4p_n^3 - 2Ap_n$$

$$\ell(p_n) = \frac{S}{\beta}\,(p_n + ik)^2 \quad , \quad \ell'(p_n) = \frac{2S}{\beta}\,(p_n + ik)$$

$$h(p_n) = (p_n + iKM)^2 + \Gamma^2 \; , \; h'(p_n) = 2(p_n + iKM) \qquad \text{(B.17)}$$

APPENDIX C

Discussion and Use of Dimensionless Parameters

The dimensionless parameters that enter into the calculation of flutter boundaries and stress estimates are summarized below together with a discussion on how to calculate dimensional quantities.

Specify whether leading and trailing edges are pinned or clamped.

$\bar{n}$ = number of half waves in the spanwise mode shape (see Appendix A)

ϵ_p, ϵ_c = degree of stringer restraint (see Appendix A) ϵ_p, ϵ_c vary between zero and unity. For pinned stringers, $\epsilon_p = 1$, $\epsilon_c = 0$ and for clamped stringers, $\epsilon_p = 0$, $\epsilon_c = 1$.

ν_x, ν_y = Poisson ratios (orthotropic constants)

Ω_{yy}, Ω_{xy} = ratios of orthotropic elastic moduli to modulus in the chordwise direction (see Eq. (1.5))

$\frac{K_e b^4}{D_{x_o}}$ = stiffness of elastic foundation ($[K_e]^*$ = lb/ft^2/ft)

$\frac{\gamma U b^3}{D_{x_o}}$ = viscous damping constant ($[\gamma]$ = lb sec/ft^3)

r_{x_o}, r_{y_o} = applied membrane stresses

r_{x_1}, r_{y_1} = nonlinear membrane stresses

r_x, r_y = $r_{x_o} + r_{x_1}$, $r_{y_o} + r_{y_1}$, respectively

Note that all of the membrane stress coefficients vary as the inverse cube of panel thickness for fixed in-plane loads (see Eq. (1.17))

M = Mach number

g = structural damping coefficient

k = reduced frequency ($\omega b/U$)

s = length-to-width ratio

*For $[K_e]$, read "dimensions of K_e"

τ = thickness-to-width ratio

R, S_o = parameters that depend on panel material, altitude, Mach number, and thickness

s_x, s_y = chordwise and spanwise dimensionless stresses

It is convenient to introduce three other parameters that are related to R and S_o, namely,

$$\mu = \frac{\rho_s \tau}{\rho_\infty}$$

$$\delta = \frac{\rho_s}{\rho_\infty}\left[\frac{\rho_\infty U^2(1 - \nu_x^2)}{2E_x}\right]^{1/3}$$

$$\eta = \frac{\rho_s a_\infty}{\rho_\infty a_s}$$

where

$$a_s = \left[\frac{E_x}{\rho_s(1 - \nu_x^2)}\right]^{1/2}$$

is the speed of longitudinal waves (sound) in the chordwise direction in the panel material. The relationship between μ, δ, η, R, and S_o is given by the following formulae:

$$\mu = \frac{R}{S_o} \qquad R = 24\frac{\delta^3}{\mu^2} = \mu S_o$$

$$\delta = \frac{R}{(24\ S_o^2)^{1/3}} \qquad S_o = 24\frac{\delta^3}{\mu^3}$$

$$\eta = \frac{1}{M}\left(\frac{S_o \mu^3}{12}\right)^{1/2} = \frac{1}{M}\sqrt{2\delta^3}$$

The dependence of each parameter on the basic physical properties (material, altitude, Mach number, and thickness) is given in Table C-1.

Table C-1. Basic Flutter Parameters

Dimensionless Parameter	Material ρ_s, a_s	Altitude ρ_∞, a_∞	Speed M	Thickness $\tau = h/b$
R	a_s^{-2}	a_∞^2	$12M^2$	τ^{-2}
S_o	$\rho_s^{-1}a_s^{-2}$	$\rho_\infty a_\infty^2$	$12M^2$	τ^{-3}
δ	$\rho_s^{2/3}a_s^{-2/3}$	$\rho_\infty^{-2/3}a_\infty^{2/3}$	$2^{-1/3}M^{2/3}$	--
μ	ρ_s	ρ_∞^{-1}	--	τ
η	$\rho_s a_s^{-1}$	$\rho_\infty^{-1}a_\infty$	--	--

To obtain an explicit formula for any dimensionless parameter, multiply out the dimensional parameters in the corresponding row.

An important point is that any two of the five parameters in Table C-1 may be used in place of R and S . A very useful pair consists of the mass ratio parameter μ and the material altitude parameter η . The advantage of this combination is that neither parameter depends on the Mach number. Thus we can display the effects of Mach number change on flutter boundaries for a given material and altitude; e.g., μ versus s plots for fixed η and different M . Conversely, we can change η at fixed Mach number and calculate the effect of a change in material or altitude. The μ,η pair is used exclusively in the present report.

The basic physical properties of various panel materials are given in Table C-2a; the variation of η with altitude for these materials is given in Table C-2b. These data are needed to calculate dimensional quantities.

Table C-2a. Material Properties at Sea Level

Material	Specific Gravity	Sound Speed ft/sec	η_o	ρ_s/ρ_{∞_o}
Aluminum	2.7	16,740	147.0	2200
Soft Steel	7.0	16,410	388.5	5700
Magnesium	1.8	15,100	106.2	1470
Nickel	8.5	16,320	478.0	6930
Copper	8.0	10,000	730.0	6515

Table C-2b. Variation of η with Altitude for Various Panel Materials

Altitude (ft)	Aluminum	Soft Steel	Magnesium	Nickel	Copper
Sea Level	147.0	388.5	106.2	478.0	730.0
5,000	167.8	444.0	121.3	544.0	833.0
10,000	192.5	509.0	139.2	625.0	955.0
20,000	256.0	677.0	185.0	831.0	1270.0
30,000	350.0	925.0	253.1	1136.0	1738.0
40,000	522.0	1380.0	378.0	1695.0	2590.0
50,000	845.0	2235.0	611.0	2741.0	4195.0

For a given flutter point, the values of μ and η are known. We now show how to calculate the panel thickness-to-width ratio τ. The first step is to prepare a graph of the density ratio $\rho_\infty/\rho_{\infty_o}$ and η versus altitude for the panel material in question. The curves for aluminum panels are given in Fig. C-1 between sea level and 50,000 ft. For given η, find the corresponding altitude and value of $\rho_\infty/\rho_{\infty_o}$ from the graph. Calculate thickness from the formula

$$\tau = \left(\frac{\rho_{\infty_o}}{\rho_s}\right) \cdot \left(\frac{\rho_\infty}{\rho_{\infty_o}}\right) \cdot \mu$$

where ρ_{∞_o}/ρ_s is obtained from Table C-2a, and μ is a given flutter point.

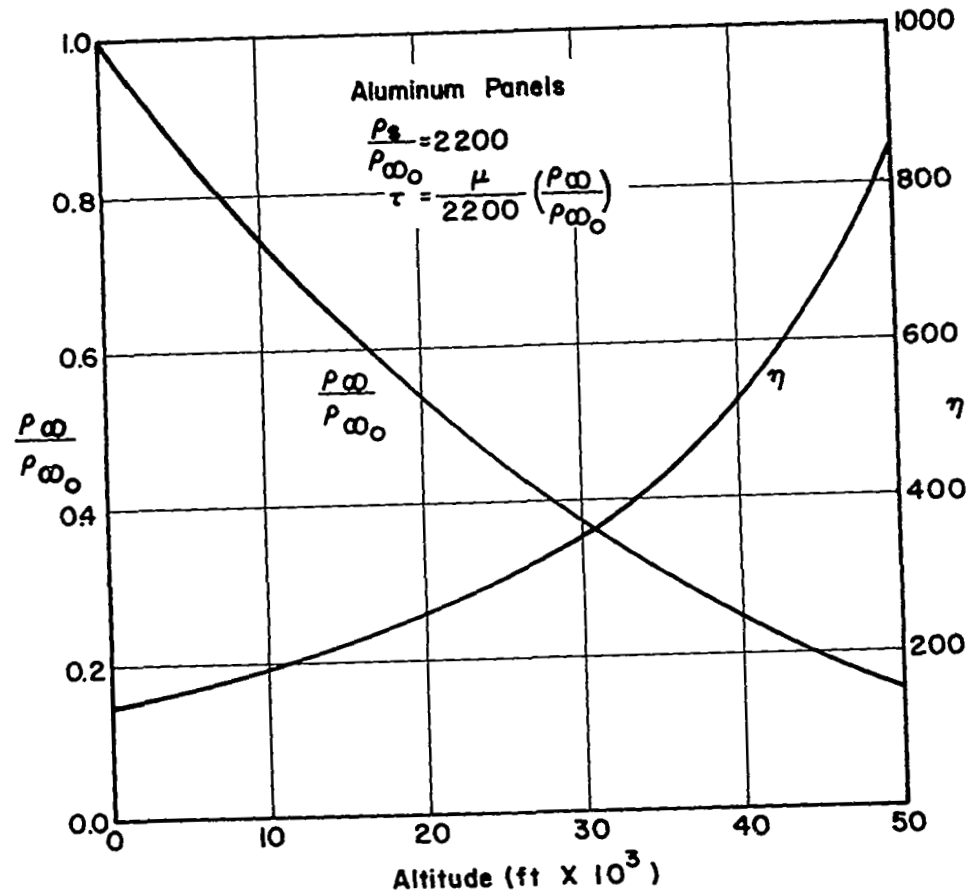

FIGURE C-1. CURVES FOR CONVERTING MASS RATIO μ TO THICKNESS τ FOR ALUMINUM PANELS AT DIFFERENT ALTITUDE; a_s = 16,740 ft/sec, ρ_s = 5.23 slugs/ft^3

REFERENCES

1. Lemley, C.E.: "Design Criteria for the Prediction and Prevention of Panel Flutter," Vol. I: Criteria Presentation, Vol. II: Background and Review of State of the Art, Tech. Rept. AFFDL-TR-67-140, August 1968.

2. Dowell, E.H.: "Panel Flutter: A Review of the Aeroelastic Stability of Plates and Shells," AIAA Jour., Vol. 8, No. 3, March 1970.

3. Garrick, I.E. and Rubinow, S.I.: "Theoretical Study of Air Forces on an Oscillating or Steady Thin Wing in a Supersonic Main Stream," NACA TN 1383, July 1947.

4. Muhlstein, L., Jr., Gaspers, P.A., Jr., and Riddle, D.W.: "An Experimental Study of the Influence of the Turbulent Boundary Layer on Panel Flutter," NASA TN D-4486, 1968.

5. Gaspers, P.A., Jr., Muhlstein, L., Jr., and Petroff, D.N.: "Further Experimental Results on the Influence of the Turbulent Boundary Layer on Panel Flutter," NASA TN D-5798, May 1970.

6. Dowell, E.H.: "Generalized Aerodynamic Forces on a Flexible Plate Undergoing Transient Motion in a Shear Flow with an Application to Panel Flutter," AIAA Paper No. 70-76, January 1970.

7. Bolotin, V.V.: Nonconservative Problems of the Theory of Elastic Stability: The Macmillan Co., New York, 1963.

8. Olson, M.D. and Fung, Y.C.: "Comparing Theory and Experiment for the Supersonic Flutter of Circular Cylindrical Shells," AIAA Jour., Vol. 5, No. 10, October 1967.

9. Dowell, E.H.: "Nonlinear Oscillations of a Fluttering Plate," AIAA Jour., Vol. 4, No. 7, July 1966.

10. Dowell, E.H.: "Nonlinear Oscillations of a Fluttering Plate, II," AIAA Jour., Vol. 5, No. 10, October 1967.

11. Eastep, F.E.: "Nonlinear Oscillations of Elastic Panels in a Supersonic Nonviscous Airstream," Stanford University SUDAAR No. 354, August 1968.

12. Zeydel, E.F.E.: "Large Deflection Panel Flutter," AFOSR Tech. Note 1952, January 1962.

13. Hedgepeth, J.N., Budiansky, B., and Leonard, R.W.: "Analysis of Flutter in Compressible Flow of a Panel on Many Supports," Jour. Aero. Sci., Vol. 21, No. 7, July 1954.

14. Houbolt, J.C.: "A Study of Several Aerothermoelastic Problems of Aircraft Structures in High-Speed Flight," Mitt. Inst. Flug Zeugstatik und Leichtban Nr. 5, Verlag Leeman, Zürich, 1958.

15. Dugundji, J.: "Theoretical Considerations of Panel Flutter at High Supersonic Mach Numbers," AIAA Jour., Vol. 4, No. 7, July 1966.

16. Zeydel, E.F.E.: "Research Study on Panel Flutter Aerodynamics," Georgia Institute of Technology, Final Report Project B-207, Contract NAS8-20100, 1967.

17. Zeydel, E.F.E. and Yates, J.E.: "Aerodynamic Forces of Fluttering Cylindrical and/or Planar Structures," Aeronautical Research Associates of Princeton, Inc. Report No. 132, March 1969.

18. Goland, M. and Luke, Y.L.: "An Exact Solution for Two-Dimensional Linear Panel Flutter at Supersonic Speeds," Jour. Aero. Sci., Vol. 21, No. 4, April 1954.

19. Conrad, P., Donaldson, C. duP., and Snedeker, R.: "A Study of the Modal Response Approach to Patterned Ablation Including Experiment Definition," Aeronautical Research Associates of Princeton, Inc. Report No. 144, April 1970.

20. Dowell, E.H.: "Flutter of Infinitely Long Plates and Shells. Part I: Plate," AIAA Jour., Vol. 4, No. 8, August 1966.

21. Dowell, E.H.: "The Flutter of Very Low Aspect Ratio Panels," AFOSR64-1723, Massachusetts Institute of Technology Aeroelastic and Structures Research Laboratory, July 1964.

22. Zeydel, E.F.E. and Kobett, D.R.: "Flutter of Flat Plates with Partially Clamped Edges in the Low Supersonic Region," AIAA Jour., Vol. 3, No. 1, January 1965.

23. Bohon, H.L. and Dixon, S.C.: "Some Recent Developments in Flutter of Flat Panels," Jour. of Aircraft, Vol. 1, No. 5, October 1964.

24. Anon., "Metallic Materials and Elements for Aerospace Vehicle Structures," MIL-HDBK-5A, February 8, 1966.

25. Fung, Y.C.: "A Summary of the Theories and Experiments on Panel Flutter," AFOSR TN 60-224, May 1960.

26. Cunningham, H.J.: "Analysis of the Flutter of Flat Rectangular Panels on the Basis of Exact Three-Dimensional Linearized Supersonic Potential Flow," AIAA Jour., Vol. 1, No. 8, August 1963.

27. "Saturn V Launch Vehicle Flight Evaluation Rept. AF-502, Apollo 6 Mission," Prepared by Saturn V Flight Evaluation Working Group, MPR-SAT-FE-68-3, June 25, 1968.

28. Luke, Y.L. and St. John, A.: "Supersonic Panel Flutter," WADC Tech. Rept. 57-252, July 1957.

29. "Handbook of Mathematical Functions with Formulas, Graphs and Mathematical Tables," edited by M. Abramowitz and I. A. Stegun, National Bureau of Standards Applied Mathematics Series 55, June 1964.

NASA-Langley, 1970 —— 32